# The effects of 17α-estradiol treatment on endocrine system revealed by single-nucleus transcriptomic sequencing of hypothalamus

Lei Li[#,*1], Guanghao Wu[#2], Xiaolei Xu[3], Junling Yang[4], Lirong Yi[5], Ziqing Yang[6], Zheng Mo[3], Li Xing[3], Ying Shan[*1], Zhuo Yu[*3], Yinchuan Li[*5]

[1]Department of Obstetrics and Gynecology, National Clinical Research Center for Obstetric & Gynecologic Diseases, Peking Union Medical College Hospital, Chinese Academy of Medical Sciences and Peking Union Medical College, 100730 Beijing, China.

[2]School of Medical Technology，Beijing Institute of Technology, 100081, Beijing, China.

[3]Department of Medical Oncology，Beijing Tsinghua Changgung Hospital, School of Clinical Medicine, Tsinghua University, 102218, Beijing, China.

[4]Department of Cancer Biology and Pharmacology, University of Illinois College of Medicine, Peoria, Illinois, United states of America.

[5]Institute of Reproductive Medicine, Medical School of Nantong University, Nantong, Jiangsu 226001, China.

[6]School of Basic Medical Sciences, Shandong University, Jinan, Shandong 250012, China.

# These authors contributed equally: Lei Li, Guanghao Wu

* Corresponding author. Email: shypumch@163.com; lilei64@pumch.cn; yza02214@btch.edu.cn; 18622397604@163.com

## Abstract

In this study, we investigated the role of 17α-estradiol in lifespan extension and its potential side effects for long-term administration. Pooled hypothalami from aged male Norway brown rats treated with 17α-estradiol (O.T), aged male controls (O), and young male controls (Y) were subjected to single-nucleus transcriptomic sequencing (snRNA-seq). To evaluate the effects of 17α-estradiol in anti-aging in neurons, supervised clustering on neurons by neuropeptides and their receptors were used to evaluate the responses of each neuron subtype during aging and after 17α-estradiol treatment. The elevated cellular metabolism, stresses and decreased synaptic activity in neurons initiated by aging were remarkably attenuated by 17α-estradiol. Assessment of changes in neuron populations showed that neurons related to food intake, reproduction, blood pressure,

stress response and electrolyte balance were sensitive to 17α-estradiol treatment. 17α-estradiol treatment not only increased Oxytocin (Oxt), but also increased the activity of hypothalamic-pituitary-gonadal (HPG) axis, evidenced by significantly elevated levels of plasma Gnrh, bioavailable testosterone, and decreased estradiol. Elevated Gnrh1 was verified to be one of the causal effects mediating the role of 17α-estradiol in energy homeostasis, neural synapse, and stress response. Notably, *Crh* neurons displayed most prominently senescent phenotype among all checked neuron subtypes in O.T, which may be a potential side effect of 17α-estradiol treatment. Therefore, HPG axis and energy metabolism may be key targets of 17α-estradiol in male lifespan extension. Additionally, supervised clustering of neurons was shown to be a useful method to assess the responses to treatment among different neuron subtypes in the hypothalamus.

**Key words** snRNA-seq, hypothalamus, 17α-estradiol, aging, Crh, Oxt, Gnrh

## Background

The hypothalamus is the central hub controlling energy homeostasis, stress response, temperature, learning, feeding, sleeping, social behavior, sexual behavior, hormone secretion, reproduction, osmoregulation, blood pressure, visceral activities, emotion, and circadian rhythms[1]. The hypothalamic energy-sensing system, especially circuits regulating food intake, is critical for life span extension [2]. Elevated metabolic activity involving many regulatory signaling pathways has been reported in aged hypothalamus, including enhanced mTor signaling [3, 4]. Decreases in gonadotropin-releasing hormone (GnRH), Ghrh, Trh, monoamine neurotransmitters, and blood supply are also hallmarks of aging hypothalamus [5].

Previous studies have shown that 17α-estradiol extends the lifespan of male mice, has beneficial effects on metabolism and inflammation with a similar mechanism as that of rapamycin and acarbose [6-8]. Further investigations revealed certain unique features of 17α-estradiol in life extension distinct to rapamycin and acarbose [9, 10]. Further, 17α-estradiol was shown to target hypothalamic *POMC* neurons to reduce metabolism by decreasing feeding behavior via anorexigenic pathways [11]. Interestingly, the lifespan extension effect is only found in male animals [12]. The safety of 17α-estradiol is key for translation into clinical treatment, and the side effects on reproduction and potential feminization by 17α-estradiol treatment need to be considered. However, contradictory results have been reported regarding its side effects on

reproduction and feminization [6, 13, 14]. A previous study showed that 17α-estradiol elicits similar genomic binding and transcriptional activation through Esr1 (estrogen receptor α, ERα) to that of 17β-estradiol, suggesting a potential side effect on reproduction and feminization [15]. Therefore, the underlying mechanism of lifespan extension and the safety of 17α-estradiol still need further investigation and verification.

In this report, we used single-nucleus transcriptomic sequencing and performed supervised clustering of neurons by neuropeptides, hormones, and their receptors. Supervised clustering provides better resolution in cell cluster screening than is achieved by traditional unsupervised clustering. The effects of 17α-estradiol on metabolism, stress responses, ferroptosis, senescence, inflammation, and synaptic activity were assessed in each neuron subtype, and the most sensitive neurons were ranked. The effects of 17α-estradiol on reversing measures of aging were evaluated by two opposing regulatory networks involved in hypermetabolism, stress, inflammation, and synaptic activity. Several key endocrine factors from serum were checked. Additionally, the potential side effects of 17α-estradiol on certain neurons were also evaluated.

## Materials and methods

### Animals, treatment and tissues

Nine Norway brown male rats were acquired from Charles River (Beijing). Aged rats were housed one per cage and young rats (1 month old) were housed two per cage. Aged rats were randomly allocated into control and 17α-estradiol-treated groups. Aged rats treated with 17α-estradiol (Catalog #: E834897, Macklin Biochemical, Shanghai, China) were fed freely with regular diet mixed with 17α-estradiol at a dose of 14.4 mg/kg (14.4 ppm), starting at 24 months of age for 6 months according to prior reports [16, 17]. The young rats were fed a regular diet without 17α-estradiol continuously for 3 months until 4 months old. All rats had ad libitum access to food and water throughout the experiments. The rats were then euthanized via $CO_2$, hypothalami, testes and blood serum were collected for subsequent experiment procedures. All blood samples were collected at 9:00-9:30 a.m to minimize hormone fluctuation between animals. All animal procedures were reviewed and approved by the Institutional Animal Care and Use Committee at Nantong University.

### Enzyme immunoassays

Enzyme immunoassays kits for rat Oxt (Catalog #: EIAR-OXT), Corticotropin Releasing Factor (Catalog #: EIAR-CRF), and gonadoliberin-1 (Catalog #: EIAR-GNRH) were obtained from Raybiotech (GA, USA). Enzyme immunoassay kits for rat serum bioavailable testosterone (Catalog #: ml002868), estradiol (Catalog #: ml002891), aldosterone (Catalog #: ml002876), and cortisol (Catalog #: ml002874) were obtained from Enzyme-linked Biotechnology (Shanghai, China). Sera from 3 animals per group were used and each was diluted 10 or 20 times for immunoassays.

**Seminiferous tubule inflammation test**

8 testes were obtained from each sample group and then subjected to fixation in 4% formalin for at least 1 week. Formalin-fixed paraffin-embedded mouse testis sections of 5 μm thickness were used for HE Staining. At least 30 seminiferous tubules in each slide were examined for inflammation test. Testis with at least 1 inflammatory seminiferous tubule was set as 1, and normal testis was set as 0 for inflammation index calculation.

**snRNA-seq data processing, batch effect correction, and cell subset annotation**

Intact hypothalami were cryopreserved in liquid nitrogen from sacrificed rats, and two to three pooled intact hypothalami from each group were homogenized in 500 μL ice-cold homogenization buffer (0.25 M sucrose, 5 mM $CaCl_2$, 3 mM $MgAc_2$, 10 mM Tris-HCl [pH 8.0], 1 mM DTT, 0.1 mM EDTA, 1× protease inhibitor, and 1 U/μL RiboLock RNase inhibitor) with Dounce homogenizer. Then, the homogenizer was washed with 700 μL ice-cold nuclei washing buffer (0.04% bovine serum albumin, 0.2 U/μL RiboLock RNase Inhibitor, 500 mM mannitol, 0.1 mM phenylmethanesulfonyl fluoride protease inhibitor in 1× phosphate buffer saline). Next, the homogenates were filtered through a 70-μm cell strainer to collect the nuclear fraction. The nuclear fraction was mixed with an equal volume of 50% iodixanol and added on top of a 30% and 33% iodixanol gradient. This solution was then centrifuged for 20 min at 10 000 ×g at 4 °C. After the myelin layer was removed from the top of the gradient, the nuclei were collected from the 30% and 33% iodixanol interface. The nuclei were resuspended in nuclear wash buffer and resuspension buffer and pelleted for 5 min at 500 ×g at 4 °C. The nuclei were filtered through a 40-μm cell strainer to remove cell debris and large clumps, and the nuclear concentration was manually assessed using trypan blue counterstaining and a hemocytometer. Finally, the nuclei were adjusted to 700–1200 nuclei/μL, and examined with a 10X Chromium platform.

Reverse transcription, cDNA amplification and library preparation were performed according to the protocol from 10X Genomics and Chromium Next GEM Single Cell 3′ Reagent Kits v3.1. Library sequencing was performed on the Illumina HiSeq™ 4000 by Gene Denovo Biotechnology Co., Ltd (Guangzhou, China).

10X Genomics Cell Ranger software (version 3.1.0) was used to convert raw BCL files to FASTQ files, and for alignment and counts quantification. Reads with low-quality barcodes and UMIs were filtered out and then mapped to the reference genome. Reads uniquely mapped to the transcriptome and intersecting an exon at least 50% were considered for UMI counting. Before quantification, the UMI sequences were corrected for sequencing errors, and valid barcodes were identified using the EmptyDrops method. The cell × gene matrices were produced via UMI counting and cell barcodes calling. Cells with an unusually high number of UMIs (≥8000) or mitochondrial gene percent (≥15%) were filtered out. Batch effect correction was performed by SCTransform function built in Seurat V4.4.0.

**Pathways, signatures, TFs and TF cofactors, cell communication**

Gene sets and pathways were derived from Hallmark gene sets of MSigDB collections, the KEGG pathway database, Reactome pathway database, and WikiPathways database, and some ontology terms derived from the Gene Ontology (GO) resource. Mitochondrial pathways were derived from MitoCarta3.0 [18]. Pathways, gene sets, and signatures were evaluated with the PercentageFeatureSet function built into R package Seurat. TFs and TF cofactors were obtained from AnimalTFDB 3.0 [19]. TFs and TF cofactors were further filtered with mean counts >0.1.

The ligand–receptor pairs were calculated via R package CommPath [20].

**Correlation analysis and ROC analysis**

Pearson correlation coefficient was calculated with the linkET package ($p < 0.05$). Fast Wilcoxon rank sum test and auROC analysis was performed with the wilcoxauc function in R package presto. The minimal cell number in either one of the comparing pairs should be no less than 15. Ranks of AUC values were in descending order. A total of 431 pathways from Hallmark, KEGG and PID databases were used for correlation analysis with MitoCarta OXPHOS subunits in neurons and non-neural cells (**Figure 2—figure supplement 1**). A total of 99 pathways related to synapse activity were derived from GO, including GO cellular components, GO biological processes and GO molecular functions (**Table S1**).

**The division of expression level-dependent clusters in each pathway and their signatures**

The quarters of the mixed cell populations from O, O.T and Y hypothalamic neurons were equally divided with R function fivenum from R package stats according to pathway expression levels. The total neurons were then divided into 4 clusters (c1-c4) accordingly. The cell proportion from O.T, O and Y neurons in each cluster were weighted against the total neurons in the 3 groups. The unique markers of each cluster were calculated with FindAllMarkers function of Seurat package. The intersection of the unique markers from 6 pathways were obtained for heatmap plotting. 19 genes highly expressed in c1 were calculated as c1.up.signature via the PercentageFeatureSet function in R package Seurat. 12 genes were highly expressed in c4 and thus were calculated as c4.up.signature. There were no intersected unique markers in cluster c2 and c3 of the 6 selected pathways.

**TF and pathway activities**

The TF resources were derived from CollecTRI, the pathway resource was from PROGENy, and the enrichment scores of TFs and pathways were performed with the Univariate Linear Model (ulm) method according to the pipeline in R package decoupleR [21].

**Subtypes of neurons generated by supervised clustering**

Subtypes of neurons were clustered by neuropeptides and receptors for neuropeptides or hormones within Neurons with the subset function from R package Seurat (the target gene expression level > 0). A total of 121 neuron subtypes were obtained, comprising 80 neuropeptide-secreting neurons and 41 neurons expressing a unique neuropeptide receptor or hormone receptor. Further groupings may exist within the identified neuron subtypes, and the category of excitatory or inhibitory neuron was not discriminated further. The cell proportion of each neuron subtype was weighted according to the total number of neurons in O.T, O, and Y samples. The mean values ± standard deviation of pathways and signatures were performed for each subtype. The top 10 and the bottom 10 items were calculated, and the top 10 subtypes ranked within each of 16 pathways or signatures were collected for word clouds annotation via R package wordcloud2.

**Differential expression and pathway enrichment analysis**

DEGs between groups were identified via FindMarkers (test.use = bimod, min.pct = 0.1, logfc. Threshold = 0.25, avg_diff > 0.1 or < −0.1). DEGs were then enriched in redundant GO terms via WebGestalt and filtered with false discovery rate <0.05 [22].

**Bidirectional Mendelian randomization (MR) study**

The protein quantitative trait locus (pQTL) GWAS summary data of 204 human endocrine-related GWAS summary data with European ancestry were obtained from open-access MRC Integrative Epidemiology Unit (IEU) (**Table S4**) [23, 24]. Independent genome-wide significant SNPs for exposure OXT (id:prot-a-2159) or GNRH1 (id: prot-a-1233) were used as instrumental variables with genome-wide significance ($P < 1 \times 10^{-5}$), independence inheritance ($r2 < 0.001$) without linkage disequilibrium (LD) with each other for MR. For the reverse MR, independent genome-wide significant SNPs from 203 endocrine-related GWAS summary data ($P < 1 \times 10^{-5}$, $r2 < 0.001$) without LD with each other were obtained as exposures and human GWAS summary data of OXT (id:prot-a-2159) or GNRH1 (id:prot-a-1233) were used as outcomes. Weak instruments less than 10 were discarded via F-statistics.

MR and reverse MR analysis were conducted with method inverse-variance weighting (IVW), MR Egger, Weighted median, Simple mode, and Weighted mode. The screening criteria: all of the odds ratio (OR) values of the 5 methods should be simultaneously either >1 or <1 and the significant p value of IVW was <0.05. The heterogeneity via IVW method and the horizontal pleiotropy were also evaluated with R package TwoSampleMR [25].

## Results

### The overall changes in aged hypothalamus with or without long-term 17α-estradiol treatment via snRNA-seq profiling

To investigate the hypothalamus as a potential key target of 17α-estradiol's effects on life extension, we performed snRNA-seq on the entire hypothalamus of aged and 17α-estradiol-treated aged Norway brown rats, and used the hypothalamus from young adult male rats as a control. We obtained 10 major cell types according to cell markers of the hypothalamus (**Figure 1A-B**). Notably, the proportions of non-neural cells were changed extensively in O (**Figure 1C**). For example, Oligo, OPC, and Micro were increased, and Astro, Tany, Fibro, PTC, and Endo were decreased in O compared with Y. The proportion of Oligo, OPC, and Micro were increased in O.T than those in Y. Endo was also increased in O.T. The proportions of Astro, Tany, Epen, and PTC were decreased more in O.T than those in O in comparison with those in Y. The results indicated that 17α-estradiol treatment had extensive effects on the proportions of non-neural cells in

hypothalamus.

Cell communication analysis indicated that the ligand–receptor pairs between neurons and other cell types also changed remarkably, such as those in Endo, Fibro, Tany, and Atro (**Figure 1D**). The significant ligand–receptor pairs among Neurons were changed in O.T and O, especially in O (**Figure 1E**). Notably, of the significant ligand–receptor pairs in neurons, *Bmp2–Acvr1/Acvr2a/Acvr2b/Bmpr*, *Gdf11–Acvr2a/Acvr2b*, *Inhba–Acvr1/Acvr2a/Acvr2b*, *Nrg1/Nrg2/Nrg4–Erbb4*, *Rspo1–Lgr5/Lrp6*, and *Rspo3–Lgr5* were exclusively and significantly increased in Neuron.O, in comparison with neurons of O.T and Y, which suggested enhanced TGF superfamily-mediated signaling activity and canonical Wnt signaling during aging. The significantly-changed ligand–receptor pairs *Nlgn1–Nrxn1/Nrxn2*, *Nlgn2–Nrxn1/Nrxn2/Nrxn3*, *Nlgn3–Nrxn1/Nrxn2/Nrxn3*, *Nxph1–Nrxn1/Nrxn2/Nrxn3*, *Nxph3–Nrxn1/Nrxn2/Nrxn3*, *Pomc–Oprd1/Oprk1/Oprm1*, and *Vip–Adcyap1r1/Avpr1a/Vipr2* were exclusively increased in neurons of O.T. These ligand–receptor pairs were related to or belonged to synaptic activity, cellular adhesion, opioid system, and vasodilation, which indicated unique roles of 17α-estradiol in restoring certain physiological functions in aging hypothalamus. The enhanced *Pomc* signal in O.T neurons is in line with prior report that 17α-estradiol treatment decreased food uptake in mice is potentially correlated with *Pomc* neurons [11].

Gene set enrichment analysis (GSEA) based on DEGs also verified the expression profiles in stress responses and synaptic activity in neurons (**Figure 1F**). ROC analysis of significantly differently expressed pathways related to neural synapse manually selected from Gene Ontology databases showed that most top-ranked pathways related to synaptic activity according to area under the curve (AUC) values were downregulated in aged neurons, and that 17α-estradiol treatment reversed this pattern (**Figure 1G, Table S1**).

Together, the findings suggested that 17α-estradiol extensively reshaped the cell populations, cellular communication, neuropeptide secretion, and neural synapse activity in aged hypothalamus, which was distinct from that of the young hypothalamus and aged hypothalamus.

**The two opposing signaling networks in regulating metabolism and synapse activity, which can be balanced effectively by 17α-estradiol**

In order to monitor the metabolism and neural status interfered by 17α-estradiol, energy

metabolism pathway MitoCarta OXPHOS subunits was used to calculate the positively- or negatively-correlated pathways in hypothalamic neurons (**Figure 2—figure supplement 1**). Energy metabolism and synapse activity was thus revealed to be two opposing regulatory signaling networks in hypothalamic neurons and 17α-estradiol strongly balanced these two opposing signaling networks (**Figure 2A**). Underlying these opposing signaling pathways were two category opposing transcriptional factors (TFs) (**Figure 2B**). For example, *Calr*, *Clu*, *Peg3*, *Prnp*, *Ndufa13*, *Actb*, *Ywhab*, *Nfe2l1*, *Mtdh*, *Npm1*, *Bex2*, *Aft4*, and *Maged1* were positively correlated with pathways in OXPHOS subunits, lysosome, protein export, mTorc1 signaling, unfolded protein response (UPR) in O, O.T and Y neurons, and were negatively correlated with pathways in ubiquitin mediated proteolysis, endocytosis, tight junction, focal adhesion, axon guidance, and MAPK signaling. Additionally, TFs *Myt1l*, *Ctnnd2*, *Tenm4*, *Camta1*, *Med12l*, *Rere*, *Csrnp3*, *Erbb4*, *Jazf1*, *Dscam*, *Klf12*, and *Kdm4c* had opposite correlation patterns with these selected pathways in O, O.T and Y neurons. These TFs may take conserved roles in regulating the two opposing biological processes in neurons of the hypothalamus.

Then, we tried to establish gene signatures to represent these two opposing signaling networks to display the cell status of aging and evaluate the effect interfered by 17α-estradiol. To accomplish this, 4 quarters (c1-c4) according to the expression level of each of the 6 selected pathways from the two opposing signaling networks were evenly divided in quantity among the mixed neurons from O, O.T and Y and the shared unique markers in each quarter were calculated (**Figure 2C, D**). From the distribution patterns we revealed that the neuron proportion decreased in O from c1 to c4 in metabolism pathways (MitoCarta OXPHOS subunits and Hallmark mTorc1 signaling), and this trend was reversed in the opposing signaling pathways (GOBP synapse organization and KEGG Mapk signaling pathway) (**Figure 2C**). But in Y this trend was on the contrary, implying the expression level of 4 quarters (c1-c4) from the two opposing signaling networks can be used to monitor the aging status. 17α-estradiol treatment alleviated this trend or even reversed the trend in O. We then screened the shared unique markers of each quarter from the 6 selected pathways to try to establish the signatures representing the two opposing signaling networks. Unique markers in c1 (19 genes, c1.up.signature) and c4 (12 genes, c4.up.signature) were obtained, but c2 and c3 didn't have unique markers shared by the 6 pathways (**Figure 2D**). Accordingly, the 19 genes in c1.up.signature displayed conversed correlation pattern with the 12 genes in c4.up.signature,

indicating the two opposing signatures are capable of reflecting the two opposing signaling networks in hypothalamic neurons (**Figure 2E**). But the two opposing signaling networks balanced by 17α-estradiol in non-neural cell types were not so striking as that in neurons, displaying variable effects on non-neurons (**Figure 2—figure supplement 2**). Therefore, in this report we mainly focused on hypothalamic neurons and its response to aging and 17α-estradiol.

**Supervised clustering revealed distinct responses of different subtypes of hypothalamic neurons to aging and 17α-estradiol**

The hypothalamus has numerous neuron subtypes that release various neuropeptides and hormones to regulate fundamental body functions. To discriminate the changes during aging and the effect of 17α-estradiol on each neuron subtype, we performed supervised clustering by neuropeptides, hormones or their receptors (**Figure 3A**). Most of the top 10 neuron subtypes in unfolded protein response (UPR), ferroptosis, mTorc1 signaling, insulin signaling pathway, immune response pathways, OXPHOS subunits, and senescence signature during aging were attenuated by 17α-estradiol treatment (**Figure 3B, Figure 3—figure supplement 1**). For example, Serpine1-secreting neurons had very high expression levels of UPR, ferroptosis signature, mTorc1 signaling, Tnfa signaling via NFKB, and OXPHOS subunit during aging that were attenuated by 17α-estradiol.

To further determine the most affected neurons in response to aging and 17α-estradiol, we calculated the frequency of each neuron subtype by combining the top 10 neurons in each of the 16 pathways and signatures (**Figure 3C, Table S2**). Serpine1-secreting neurons were enriched exclusively in aged hypothalamus, suggesting this type of neuron was an effective target of 17α-estradiol. Additionally, *Mlnr*, *Nmb*, *Pomc*, *Ednra*, *Serpine3*, *Gast*, and *Pcsk6* neurons were all affected by 17α-estradiol (**Figure 3D**). *Galp*, *Glp1r*, *Serping1*, *Sstr2*, *Sstr3*, and *Vip* neurons were enriched in O, O.T and Y hypothalamus, suggesting a lack of effect of 17α-estradiol on these neuron types. The unique neurons in O.T (*Crh*, *Serpinb9*, *Cckbr*, *Pth2r*, *Kiss1*, *Prpr*, *Hcrtr1*, *Npb*, *Nppa*, *Nxph3*, and *Npff*) may be the consequence of side effects or compensatory effects by 17α-estradiol treatment.

We then evaluated the most and the least affected neurons by aging via ranking the neuron subtypes according to the levels of c1.up.signature and c4.up.signature (**Figure 3E**). *Serpine1*,

*Galp*, *Calca* neurons were among the most affected neuron subtypes in aged hypothalamus which was similar to the combined ranks of several pathways (**Figure 3—figure supplement 1**). *Npr3*, *Crh*, *Ar*, *Esr1*, and *Esr2* neurons were among the least affected neuron subtypes in aged hypothalamus (**Figure 3E**). The neuron subtypes ranked by c1.up.signature and c4.up.signature in O.T indicated that neurons *Gast*, *Npb*, *Nppa*, and *Crh* were affected most by the treatment of 17α-estradiol (**Figure 3F**). And neurons *Oxtr*, *Glp1r*, *Gnrh1*, and *Crh* also showed lowest levels of c4.up.signature, indicative of aging phenotype. Meanwhile, neurons *Glp2r*, *Ar* and *Esr1* were among the top ranked neurons by the level of c4.up.signature indicating higher synapse activities and relatively less stress status in these types of neurons in O.T.

These results indicated that supervised clustering of each subtype of neurons facilitated the visualization of different subtypes of neurons in response to aging and medical treatments. Additionally, it also strongly suggested that *Crh*, *Oxtr*, *Glp1r*, *Gnrh1*, *Glp2r*, *Ar*, and *Esr1* neuron subtypes were most sensitive to long-term 17α-estradiol treatment, which were associated with appetite, glucose metabolism, stress, and sex hormone secretion and signaling.

**The potential side effects on hypothalamic–pituitary–adrenal (HPA) axis by long-term 17α-estradiol treatment in the males**

To further investigate the potential side effect or compensatory effect of 17α-estradiol treatment, we performed stricter screening by intersection of the top 10 ranks in UPR, OXPHOS subunits, and ferroptosis signature (**Figure 4A**). *Crh* and *Nppa* were the only two intersected neuron subtypes with this strict screening. 17α-estradiol elevated several key metabolic pathways in *Crh* neurons comparing with that in Y and O (**Figure 4B**). 17α-estradiol treatment also increased c1-up-signature, and at the same time lowered many pathways associated with synapse activity and c4-up-signature in *Crh* neurons of O.T, indicative of senescent phenotype in *Crh* neuron. But in *Nppa* and *Nppc* neurons, decreased c1-up-signature in O.T implied lesser extent of senescent phenotype in these neurons than *Crh* neurons. The senescence of *Crh* neurons was also verified by the increased number of DEGs of mitochondria-expressed genes in O.T and lowered the number of DEGs in pathway adherens junction (**Figure 4C**). The status of Crh neurons in O.T may be associated with the elevated TF activities of *Esr2*, *Usf2*, *Hdac5*, *Creb3l1*, *Tfam*, *Preb*, *Pou3f2*, and *Hoxb5* (**Figure 4D**).

Notably, the HPA axis was altered by 17α-estradiol treatment as evidenced by the elevated cortisol in O.T comparing with O (p = 0.078) (**Figure 4E**). The correlation of the elevated cortisol production and the increased senescence in *Crh* neurons by 17α-estradiol treatment needs further investigation. Additionally, as a key knot of renin-angiotensin-aldosterone system, the significantly increased serum aldosterone in O.T and its potential role in sodium reabsorption and cardiovascular fitness also needs further detailed investigation (**Figure 4E**).

In summary, 17α-estradiol treatment changed the activity of HPA axis in male BN rats and also brought increased potential side effects to *Crh* neuron.

**17α-estradiol increased Oxt neuron proportion and secretion and its possible role in mediating the effect of 17α-estradiol on endocrine system**

Aging and 17α-estradiol treatment also changed the proportions of various neuron subtypes among O, O.T and Y (**Figure 5A, B, Table S3**). The proportions of *Grp*, *Pmch*, *Npb*, *Serpinb9*, *Sstr2*, *Agrp*, *Sstr3*, *Mlnr*, and *Hcrt* neurons ranked in the top 10 in O, and *Oxt*, *Vip*, *Avp*, *Calca*, *Glp2r*, *Tacr1*, *Trh*, *Serping1*, *Npff*, and *Npy1r* were in the top 10 in O.T. *Galp*, *Calcrl*, *Ednra*, *Oxt*, *Serpinh1*, *Pomc*, *Cck*, *Crh*, *Tacr1*, and *Kiss1* neurons were the bottom 10 neurons in O, and *Oxtr*, *Galp*, *Agrp*, *Serpinb9*, *Npvf*, *Serpinh1*, *Ednrb*, *Agt*, *Gipr*, and *Pomc* neurons were the bottom 10 in O.T. *Agrp*, *Pomc*, *Oxt*, *Oxtr*, *Gipr*, and *Glp2r* neurons are well-known for their roles in regulating food intake and energy homeostasis. *Agrp* neurons are activated upon hunger and *Pomc* neurons are activated by satiety in the ARC of the hypothalamus. 17α-estradiol treatment effectively elevated the expression profiles of the c4.up.signature and synapse activities in neuron subtypes *Agrp*, *Pomc*, *Oxt* and *Glp2r* in O.T in comparison with O, which may relieve the adverse effects of reduced cell populations in Pomc and *Agrp* neurons in aging hypothalamus (**Figure 5C**), which indicated a potential role of 17α-estradiol in appetite control, as has been previously reported [11]. Additionally, 17α-estradiol treatment resulted in elevated proportions of *Vip*, *Avp*, *Npff*, *Calca*, and *Tacr1* neurons, which ranked in the top 10, and decreased proportions of *Agt* neurons, all of which are associated with blood pressure regulation (**Figure 5—figure supplement 1**). Notably, the proportions of *Oxt* neurons and *Glp2r* neurons, two types of neurons with anorexigenic effects [26, 27], were increased in O.T. In addition to the increased number of *Oxt*-positive neurons, the expression level of *Oxt* was also increased in O.T. The elevated synapse activities were also

evidenced by the increased DEGs in enriched pathway synaptic membrane in *Oxt* neurons (**Figure 5D**). More importantly, serum level of Oxt was significantly elevated in O.T in comparison with O (p=0.04), though its level was still lower than that of Y (**Figure 5E**). Unfortunately, the top TF activities in O.T and O were much different from those in Y (**Figure 5F**). The elevated *Hopx* and *Xbp1* may be associated with the response to 17α-estradiol treatment.

Due to the intricate regulatory networks between various endocrine factors, the elucidation of the causal effect of Oxt on other endocrine factors is thus very complicate through traditional methods. MR analysis with variant SNPs as genetic tools has much advantageous in such task. We thus performed bidirectional MR analysis of the GWAS summary data of human plasma OXT and 203 endocrine-related and hypothalamus-related factors, most of which are protein quantitative trait loci (pQTL) data from IEU (**Table S4**). As an exposure, OXT was revealed to be the significant causal effect on POMC/beta-endorphin (id:prot-a-2327, id:prot-a-2325), glucagon (id:prot-a-1181), GNRH1/Progonadoliberin-1 (id:prot-a-1233) and total testosterone levels (id:ebi−a−GCST90012112, id:ieu−b−4864) (**Figure 5G**). NPW and CBLN1 were found to be negatively associated with OXT. The significance of these significant associations was not found in the reverse MR analysis (**Figure 5—figure supplement 2A, B**). Unfortunately, we were unable to screen significant associations between OXT and estradiol levels (id:ebi-a-GCST90012105, id:ebi-a-GCST90020092, id:ebi-a-GCST90020091, id:ieu-b-4872, id:ieu-b-4873, id:ukb-e-30800_AFR, id:ukb-e-30800_CSA). Interestingly, QRFP, IGF1, AGRP, TAC4, GRP, CLU, BNF, PCSK7, PACAP, ANP, TAC3, CRH, INSL6, and PRL displayed significant associations with OXT in both MR and reverse MR, indicative of their complicate causal effects (**Figure 5—figure supplement 2A, B**). The results suggested that elevated Oxt levels induced by 17α-estradiol may have positive associations with endocrine factors governing feeding behavior, glucose metabolism, male reproduction, and sex hormones. Therefore, OXT was a potential mediator of 17α-estradiol.

**17α-estradiol activated HPG axis and the elevated Gnrh also took important roles in mediating the effect of 17α-estradiol on other endocrine factors**

Since Gnrh and sex hormone expressed neuron subtypes were sensitive to 17α-estradiol treatment (**Figure 3F, Figure 3—figure supplement 1**), we then checked their expression profile with

representative pathways of two opposing signaling networks of metabolism and synapse, including c1-up-signature and c4-up-signature (**Figure 6A**). But both c1-up-signature and c4-up-signature were not up-regulated in *Gnrh1* neuron in O.T, which was similar to *Esr2* neuron. Only in *Esr1* neuron, the c1-up-signature was up-regulated. Meanwhile, both *Ar* and *Esr* neurons also displayed high level of c4-up-signature, indicative of relatively healthy status. The data implied that most of the 4 types of sex hormone-related neurons didn't experience severe aging in O.T. However, from these expression profile, it's hard to define the exact physiological status of these subtype of neurons, especially neural endocrine activities. Therefore, we further performed enzyme immunoassays of hormones from the serum of O, O.T and Y. 17α-estradiol treatment significantly increased the plasma level of Gnrh in comparison with Y ($p = 0.0099$) and O ($p = 0.096$) (**Figure 6B**). More interestingly, testosterone level in serum was significantly increased in O.T in comparison with O ($p = 0.018$) and Y ($p = 0.052$). Meanwhile, the serum level of estradiol was significantly increased in O comparing with Y ($p = 0.011$) and significantly decreased in O.T in comparison with O ($p = 0.019$), suggesting 17α-estradiol treatment strongly altered the homeostasis of testosterone and estradiol. Additionally, most testes from 30-month-old male BN rats experienced severe age-related inflammation and epithelial collapse of seminiferous tubules (**Figure 6C**). The testes without inflammation in O.T displayed normal morphology. 17α-estradiol treatment slightly decreased the testis inflammation in O.T in comparison with that in O ($p = 0.15$), indicating a positive role of 17α-estradiol treatment in male reproductive system. Additionally, the elevated transcriptional factors as *Sf1*, *Pparg*, *Litaf*, *Nupr1*, *Rxrg*, *E2f2*, and *Zfp42* may be involved in the transcriptional regulation by 17α-estradiol in O.T (**Figure 6D**). More importantly, both the activities of androgen and estrogen pathways were decreased in *Gnrh1* neurons in O.T comparing with O and distinct to those in *Ar*, *Esr1*, and *Esr2* neurons (**Figure 6E**). These signaling is important for the feedback controlling of sex hormone secretion in *Gnrh* neurons. This result may also reflect the strong effect of 17α-estradiol on *Gnrh* neurons.

To decipher the potential effects of elevated serum Gnrh levels on endocrine system, we performed bidirectional MR analysis of the GWAS summary data of human GNRH1 (id: prot-a-1233) and 203 endocrine-related factors with genetic variants SNPs. The strong causal effects of GNRH1 on GAL/Galanin (id:prot−a−1166), POMC/Beta−endorphin (id:prot−a−2327, id:prot−a−2325), Adrenomedullin (id:prot−a−48), BDNF (id:prot−a−242)**,** and LPR

(id:prot−a−1724), which are involved in feeding, energy homeostasis, osmotic regulation , and neuron plasticity (**Figure 6F**). Notably, CRH/Corticotropin (id:prot−a−2326), PRLH/Prolactin−releasing peptide (id:prot−a−2376), NPW/Neuropeptide W (id:prot−a−2082), Glucagon (id:prot−a−1181), Chromogranin−A (id:prot−a−538) displayed bidirectional significance, indicating close and complicated causal effects between GNRH1 and these endocrine factors (**Figure 6G, Figure 6—figure supplement 1A, B**). These results also suggested that the role of 17α-estradiol treatment in feeding, energy homeostasis, reproduction, osmotic regulation, stress response, and neuron plasticity may be mediated at least by elevated Gnrh secretion.

## Discussion

The most striking role of 17α-estradiol treatment revealed in this study showed that HPG axis was substantially improved. The underlying molecular mechanism is still unknown. But prior report indicated that 17α-estradiol is able to bind ESR1 [15]. In this report, 17α-estradiol treatment significantly decreased serum estradiol and elevated serum testosterone. Combining these information, we propose 17α-estradiol may have similar roles of estrogen antagonists or the roles of aromatase inhibitors, which may prevent the conversion of androgens to estrogens [28, 29]. These roles can remove the feedback inhibition by estrogen on hypothalamus and pituitary to secret Gnrh, FSH, and LH [30].

The testosterone levels declined gradually from the third decade of life in men [31]. Ageing of the gonadotropic axis, especially aged males with low serum testosterone, is usually associated with many aging symptoms as the age-related loss of skeletal muscle mass, muscle strength, muscle power, low bone mineral density, frailty, impaired physical performance, mobility limitation, increased risk of diabetes, higher all-cause mortality and cardiovascular mortality, cognitive decline, and increased risk of Alzheimer’s disease [32]. Therefore, testosterone supplementation to older men is benefit. Additionally, Gnrh supplement alleviates aging-impaired neurogenesis and thus decelerates aging [33]. 17α-estradiol treatment didn’t lead to feminization and didn’t affect the sperm parameter, fertility in male animals [6, 13]. Therefore, the increased Gnrh levels and serum testosterone by 17α-estradiol treatment is likely benefit to older males especially to those with syndrome of late-onset hypogonadism.

Similar aging syndrome to aged males with low serum testosterone, postmenopausal women with

low estrogen also experience increased mortality, cardiovascular disease, osteoporosis fracture, urogenital atrophy and dementia, which are also benefit from hormone therapy [34]. But why 17α-estradiol treatment doesn't display positive life extension roles in aged females according to prior report [12]? The underlying key point may be the inhibition of estrogens by 17α-estradiol treatment. This is also evidenced by the inability of 17α-estradiol to improve female fertility [35]. However, due to lacking parallel data in aged female BN rats treated with 17α-estradiol, the exact answer to this question needs more investigation in the females in the future.

Another striking effect of 17α-estradiol to hypothalamus neurons was to decrease the overall energy metabolism in aged male BN rats. The nutrient-sensing network, mediated by MTORC1 complex, is a central regulator of mRNA and ribosome biogenesis, protein synthesis, glucose, autophagy, lipid metabolism, mitochondrial biosynthesis, and proteasomal activity [36]. Downregulation of the nutrient-sensing network can increase lifespan and healthspan [37]. 17α-estradiol treatment attenuated nutrient-sensing network activity in most hypothalamic neurons, which promoted lifespan extension. Additionally, synaptic aging leads to a decline of synaptic activity and estrogen improves the performance of aging synapses [38]. In line with this, our data showed that the benefit of improved synaptic activity by 17α-estradiol treatment was prominent in aging male hypothalamus.

In this report, we showed that neuron populations in appetite control, specifically *Agrp*, *Pomc*, *Oxt*, *Oxtr*, *Gipr*, and *Glp2r* neurons, were extensively changed. The Oxt neuron proportion was elevated the most by 17α-estradiol in all detected neuron subtypes (**Figure 5A**). Oxt plays versatile roles in social behavior, stress response, satiety, energy balance, reproduction, and inflammation [39]. Most *Oxt* neurons are produced by the PVN and supraoptic nuclei (SON) in hypothalamus with very high plasticity during development and intricate circuits [40, 41]. PVN, ARC, and ventromedial hypothalamic nucleus compose the neural hub in the hypothalamus that integrates peripheral, nutritional, and metabolic signals to control food intake behavior and energy balance [42]. Many effects of Oxt are sex-specific [43]. For example, females are less sensitive to exogenous Oxt than males in social recognition [44]. More interestingly, Oxt injection, which was delivered via improved blood–brain barrier penetration nanoparticles, decreased body mass, and increased social investigation and Oxt-positive cell number in the SON of hypothalamus preferentially in male rats [45]. Intracerebroventricular Oxt injection in rats showed that food

intake was reduced in both sexes with a more pronounced effect in males [46].Therefore, we propose that the role of Oxt in systemic aging and feeding behavior is another potential contributing factor in mediating the sex-biased effects of 17α-estradiol.

17α-estradiol treatment apparently induced elevated aging of HPA axis. One evidence was the increased senescence of *Crh* neurons. The other evidence was the elevated serum cortisol, which is a hallmark of aging HPA axis [47, 48]. Therefore, more attentions should be paid to the potential side effects of 17α-estradiol especially in its clinical application.

Together, the findings suggest that HPG axis and neurons involved in appetite and energy balance were improved by 17α-estradiol treatment, which may be closely related to the life-extension roles of 17α-estradiol in aged males. Additionally, supervised clustering by neuropeptides, hormones and their receptors is proved to be a useful strategy to investigate the pharmacological, pathological and physiological processes in each subtype of neurons in the hypothalamus.

**Abbreviations**

Ar: androgen receptor; ARC: arcuate nucleus; Astro: astrocyte; AUC: area under the curve; Cga: glycoprotein hormones, alpha Polypeptide; Crh: corticotropin releasing hormone; DEG: differentially-expressed gene; Endo: endothelial cell; Esr1: estrogen receptor 1; Esr2: estrogen receptor 2; Fibro: fibroblast; Glp2r: glucagon-like peptide 2 receptor; GnRH: gonadotropin releasing hormone; GSEA: gene set enrichment analysis; HPA: hypothalamic–pituitary–adrenal**;** HPG: hypothalamic-pituitary-gonadal; IEU: MRC Integrative Epidemiology Unit; IVW: inverse-variance weighting; KEGG: Kyoto Encyclopedia of Genes and Genomes; Micro: microglia; MR: Mendelian randomization; MTORC1: mechanistic target of rapamycin kinase 1; Nppa: natriuretic peptide A; Oligo: oligodendrocyte; OPC: oligodendrocyte precursor cell; OR: odds ratio; OXPHOS: oxidative phosphorylation; PID: Pathway Interaction Database; POMC: proopiomelanocortin; pQTL: protein quantitative trait loci; PTC: pars tuberalis cell; PVN: paraventricular nucleus; ROC: receiver operating characteristics; snRNA-seq: single-nucleus transcriptomic sequencing; Tany: tanycyte; TF: transcription factor; UPR: unfolded protein response.

**Acknowledgments**

We appreciate Dr. Qinghua Wang and Hongyun Shi from animal facility of Nantong University in

helping with the animal experiments. Special thanks to Professor Ken-ichiro Fukuchi from University of Illinois College of Medicine for constructive comments and suggestions in manuscript preparation.

**Funding:** This work was supported by the National Natural Science Foundation of China grant 31271448 (YL), 82171621 (LL), 82172566 (ZY), 82150107 (RL) and the National High Level Hospital Clinical Research Funding (2022-PUMCH-A-231) (LL).

**Author contributions:** Conceptualization, YL, LL; Methodology, YL, GW, XX; Animal operation: YL, LL; EIA assays: YL, LY; Inflammation test: YL, ZY, LL, YS. Validation, LL, JY, ZY; Formal Analysis, YL, JY; Resources, GW, YS, ZY, ZM, LX; Visualization, YL; Writing – Original Draft, YL, JY; Writing – Review & Editing, LL, YS; Supervision, YS, ZY, YL; Project Administration, YL, ZY, LL; Funding Acquisition, ZY, LL. All authors have read and approved the final manuscript.

**Declaration of competing interest**

The authors have no conflict of interests to declare.

**Availability of data and materials**: All data are available at GEO accession number GSE248413.

**Competing interests**

All authors declare no competing interests.

**References**

1. Hajdarovic KH, Yu D, Webb AE. Understanding the aging hypothalamus, one cell at a time. Trends Neurosci. 2022; 45: 942-54.

2. Dacks PA, Moreno CL, Kim ES, Marcellino BK, Mobbs CV. Role of the hypothalamus in mediating protective effects of dietary restriction during aging. Front Neuroendocrinol. 2013; 34: 95-106.

3. Masliukov PM. Changes of Signaling Pathways in Hypothalamic Neurons with Aging. Curr Issues Mol Biol. 2023; 45: 8289-308.

4. Yang SB, Tien AC, Boddupalli G, Xu AW, Jan YN, Jan LY. Rapamycin ameliorates age-dependent obesity associated with increased mTOR signaling in hypothalamic POMC neurons. Neuron. 2012; 75: 425-36.

5. Yang H, Fang B, Wang Z, Chen Y, Dong Y. The Timing Sequence and Mechanism of Aging in

Endocrine Organs. Cells. 2023; 12.

6. Stout MB, Steyn FJ, Jurczak MJ, Camporez JG, Zhu Y, Hawse JR, et al. 17α-Estradiol Alleviates Age-related Metabolic and Inflammatory Dysfunction in Male Mice Without Inducing Feminization. J Gerontol A Biol Sci Med Sci. 2017; 72: 3-15.

7. Shen Z, Hinson A, Miller RA, Garcia GG. Cap-independent translation: A shared mechanism for lifespan extension by rapamycin, acarbose, and 17α-estradiol. Aging Cell. 2021; 20: e13345.

8. Wink L, Miller RA, Garcia GG. Rapamycin, Acarbose and 17α-estradiol share common mechanisms regulating the MAPK pathways involved in intracellular signaling and inflammation. Immun Ageing. 2022; 19: 8.

9. Watanabe K, Wilmanski T, Baloni P, Robinson M, Garcia GG, Hoopmann MR, et al. Lifespan-extending interventions induce consistent patterns of fatty acid oxidation in mouse livers. Commun Biol. 2023; 6: 768.

10. Burns AR, Wiedrick J, Feryn A, Maes M, Midha MK, Baxter DH, et al. Proteomic changes induced by longevity-promoting interventions in mice. Geroscience. 2024; 46: 1543-60.

11. Steyn FJ, Ngo ST, Chen VP, Bailey-Downs LC, Xie TY, Ghadami M, et al. 17α-estradiol acts through hypothalamic pro-opiomelanocortin expressing neurons to reduce feeding behavior. Aging Cell. 2018; 17.

12. Harrison DE, Strong R, Allison DB, Ames BN, Astle CM, Atamna H, et al. Acarbose, 17-α-estradiol, and nordihydroguaiaretic acid extend mouse lifespan preferentially in males. Aging Cell. 2014; 13: 273-82.

13. Isola JVV, Veiga GB, de Brito CRC, Alvarado-Rincón JA, Garcia DN, Zanini BM, et al. 17α-estradiol does not adversely affect sperm parameters or fertility in male mice: implications for reproduction-longevity trade-offs. Geroscience. 2023; 45: 2109-20.

14. Stout MB, Vaughan KL, Isola JVV, Mann SN, Wellman B, Hoffman JM, et al. Assessing tolerability and physiological responses to 17α-estradiol administration in male rhesus macaques. Geroscience. 2023; 45: 2337-49.

15. Mann SN, Hadad N, Nelson Holte M, Rothman AR, Sathiaseelan R, Ali Mondal S, et al. Health benefits attributed to 17α-estradiol, a lifespan-extending compound, are mediated through estrogen receptor α. Elife. 2020; 9.

16. Harrison DE, Strong R, Reifsnyder P, Kumar N, Fernandez E, Flurkey K, et al. 17-a-estradiol late

in life extends lifespan in aging UM-HET3 male mice; nicotinamide riboside and three other drugs do not affect lifespan in either sex. Aging Cell. 2021; 20: e13328.

17. Strong R, Miller RA, Antebi A, Astle CM, Bogue M, Denzel MS, et al. Longer lifespan in male mice treated with a weakly estrogenic agonist, an antioxidant, an α-glucosidase inhibitor or a Nrf2-inducer. Aging Cell. 2016; 15: 872-84.

18. Rath S, Sharma R, Gupta R, Ast T, Chan C, Durham TJ, et al. MitoCarta3.0: an updated mitochondrial proteome now with sub-organelle localization and pathway annotations. Nucleic Acids Res. 2021; 49: D1541-d7.

19. Hu H, Miao YR, Jia LH, Yu QY, Zhang Q, Guo AY. AnimalTFDB 3.0: a comprehensive resource for annotation and prediction of animal transcription factors. Nucleic Acids Res. 2019; 47: D33-d8.

20. Lu H, Ping J, Zhou G, Zhao Z, Gao W, Jiang Y, et al. CommPath: An R package for inference and analysis of pathway-mediated cell-cell communication chain from single-cell transcriptomics. Comput Struct Biotechnol J. 2022; 20: 5978-83.

21. Badia IMP, Vélez Santiago J, Braunger J, Geiss C, Dimitrov D, Müller-Dott S, et al. decoupleR: ensemble of computational methods to infer biological activities from omics data. Bioinform Adv. 2022; 2: vbac016.

22. Liao Y, Wang J, Jaehnig EJ, Shi Z, Zhang B. WebGestalt 2019: gene set analysis toolkit with revamped UIs and APIs. Nucleic Acids Res. 2019; 47: W199-w205.

23. Hemani G, Zheng J, Elsworth B, Wade KH, Haberland V, Baird D, et al. The MR-Base platform supports systematic causal inference across the human phenome. Elife. 2018; 7.

24. Sun BB, Maranville JC, Peters JE, Stacey D, Staley JR, Blackshaw J, et al. Genomic atlas of the human plasma proteome. Nature. 2018; 558: 73-9.

25. Hemani G, Tilling K, Davey Smith G. Orienting the causal relationship between imprecisely measured traits using GWAS summary data. PLoS Genet. 2017; 13: e1007081.

26. Inada K, Tsujimoto K, Yoshida M, Nishimori K, Miyamichi K. Oxytocin signaling in the posterior hypothalamus prevents hyperphagic obesity in mice. Elife. 2022; 11.

27. Dalvi PS, Belsham DD. Glucagon-like peptide-2 directly regulates hypothalamic neurons expressing neuropeptides linked to appetite control in vivo and in vitro. Endocrinology. 2012; 153: 2385-97.

28. Leder BZ, Rohrer JL, Rubin SD, Gallo J, Longcope C. Effects of aromatase inhibition in elderly

men with low or borderline-low serum testosterone levels. J Clin Endocrinol Metab. 2004; 89: 1174-80.

29. Guay AT, Jacobson J, Perez JB, Hodge MB, Velasquez E. Clomiphene increases free testosterone levels in men with both secondary hypogonadism and erectile dysfunction: who does and does not benefit? Int J Impot Res. 2003; 15: 156-65.

30. Wang C, Swerdloff RS. Testosterone Replacement Therapy in Hypogonadal Men. Endocrinol Metab Clin North Am. 2022; 51: 77-98.

31. Camacho EM, Huhtaniemi IT, O'Neill TW, Finn JD, Pye SR, Lee DM, et al. Age-associated changes in hypothalamic-pituitary-testicular function in middle-aged and older men are modified by weight change and lifestyle factors: longitudinal results from the European Male Ageing Study. Eur J Endocrinol. 2013; 168: 445-55.

32. Rodrigues Dos Santos M, Bhasin S. Benefits and Risks of Testosterone Treatment in Men with Age-Related Decline in Testosterone. Annu Rev Med. 2021; 72: 75-91.

33. Zhang G, Li J, Purkayastha S, Tang Y, Zhang H, Yin Y, et al. Hypothalamic programming of systemic ageing involving IKK-β, NF-κB and GnRH. Nature. 2013; 497: 211-6.

34. Shoupe D. Individualizing hormone therapy to minimize risk: accurate assessment of risks and benefits. Womens Health (Lond). 2011; 7: 475-85.

35. Isola JVV, Zanini BM, Hense JD, Alvarado-Rincón JA, Garcia DN, Pereira GC, et al. Mild calorie restriction, but not 17α-estradiol, extends ovarian reserve and fertility in female mice. Exp Gerontol. 2022; 159: 111669.

36. López-Otín C, Blasco MA, Partridge L, Serrano M, Kroemer G. Hallmarks of aging: An expanding universe. Cell. 2023; 186: 243-78.

37. Singh PP, Demmitt BA, Nath RD, Brunet A. The Genetics of Aging: A Vertebrate Perspective. Cell. 2019; 177: 200-20.

38. Morrison JH, Baxter MG. The ageing cortical synapse: hallmarks and implications for cognitive decline. Nat Rev Neurosci. 2012; 13: 240-50.

39. Kerem L, Lawson EA. The Effects of Oxytocin on Appetite Regulation, Food Intake and Metabolism in Humans. Int J Mol Sci. 2021; 22.

40. Rosen GJ, de Vries GJ, Goldman SL, Goldman BD, Forger NG. Distribution of oxytocin in the brain of a eusocial rodent. Neuroscience. 2008; 155: 809-17.

41. Madrigal MP, Jurado S. Specification of oxytocinergic and vasopressinergic circuits in the developing mouse brain. Commun Biol. 2021; 4: 586.

42. Cornejo MP, Hentges ST, Maliqueo M, Coirini H, Becu-Villalobos D, Elias CF. Neuroendocrine Regulation of Metabolism. J Neuroendocrinol. 2016; 28.

43. Carvalho Silva R, Pisanu C, Maffioletti E, Menesello V, Bortolomasi M, Gennarelli M, et al. Biological markers of sex-based differences in major depressive disorder and in antidepressant response. Eur Neuropsychopharmacol. 2023; 76: 89-107.

44. Dumais KM, Veenema AH. Vasopressin and oxytocin receptor systems in the brain: Sex differences and sex-specific regulation of social behavior. Front Neuroendocrinol. 2016; 40: 1-23.

45. Duarte-Guterman P, Lieblich SE, Qiu W, Splinter JEJ, Go KA, Casanueva-Reimon L, et al. Oxytocin has sex-specific effects on social behaviour and hypothalamic oxytocin immunoreactive cells but not hippocampal neurogenesis in adult rats. Horm Behav. 2020; 122: 104734.

46. Liu CM, Davis EA, Suarez AN, Wood RI, Noble EE, Kanoski SE. Sex Differences and Estrous Influences on Oxytocin Control of Food Intake. Neuroscience. 2020; 447: 63-73.

47. Veldhuis JD. Changes in pituitary function with ageing and implications for patient care. Nat Rev Endocrinol. 2013; 9: 205-15.

48. Warde KM, Smith LJ, Basham KJ. Age-related Changes in the Adrenal Cortex: Insights and Implications. J Endocr Soc. 2023; 7: bvad097.

## Figure legends

**Figure 1. snRNA-seq profiling of the hypothalamus from O, O.T and Y samples. (A)** UMAP visualization of nuclei colored by 10 cell types: neuron (Neu), astrocyte (Astro), oligodendrocyte (Oligo), oligodendrocyte precursor cell (OPC), tanycyte (Tany), ependymocyte (Epen), microglia (Micro), fibroblast (Fibro), pars tuberalis cell (PTC), and endothelial cell (Endo), from hypothalamus of aged rats (O), 17α-estradiol-treated aged rats (O.T) and young rats (Y). **(B)** Heatmap showing the classic markers of 10 major cell types in hypothalamus. **(C)** Cell-type compositions by groups (left panel) or by major cell types with the total cell numbers shown above each column. **(D)** Circos plot depicting the number of ligand–receptor pairs between Neu and other cell types (color strips) for each group. **(E)** Dot plot showing significant ligand–receptor interactions between Neurons for each group. Boxes showing the unique ligand–receptor

interactions between Neuron.O (black boxes) or between Neuron.O.T (blue boxes). **(F)** Dot plot of enriched GO biological process terms across three groups of neurons via GSEA analysis. **(G)** The top 15 changed pathways/gene sets according to the ranks of AUC values in selected pathways related to neuronal synapses and axons from Gene Ontology (GO) biological process, GO molecular function and GO cellular component.

**Figure 2. Two opposing regulatory signaling networks in neuron metabolism. (A)** Dot plot of the selected pathways representing the prominent changes of overall expression levels across Neuron.O, Neuron.O.T and Neuron.Y in metabolism, signaling and synaptic activity. **(B)** Correlation heatmap showing transcription factors (TFs) that correlated with the two opposing regulatory signaling networks in the mixed neurons of O, O.T and Y. **(C)** The shared unique markers of each quarter (c1-c4) in 6 pathways in hypothalamic neurons (O, O.T, and Y). The markers were then collected as c1.up.signature (19 genes) and c4.up.signature (12 genes). **(D)** The aging-related cell proportions of each quarter shown by 4 pathways. **(E)** The correlation of c1.up.signature and c2.up.signature with the two opposing regulatory signaling networks.

**Figure 3. Screening of neuron subtypes by supervised clustering that responded distinctly to aging and 17α-estradiol treatment. (A)** Diagram outlining the features of supervised clustering of neurons in hypothalamus compared with the traditional unsupervised clustering. **(B)** The top 10 and bottom 10 neurons of 121 neurons according to the mean expression values of eight signaling pathways from stress, apoptosis, metabolism, immune response, and senescence in Neuron.O. The expression levels of these neuron subtypes from Neuron.O.T and Neuron.Y were also indicated. **(C)** Word clouds displaying the frequency of neurons that were among the top 10 in each of the 16 signaling pathways as shown in **Table S2**. The 16 pathways were from oxidative stress, apoptosis, metabolism, immune response, and senescence. **(D)** Venn diagram showing the number of neuron subtypes exclusively in each group or shared by the groups in (C). The neurons with frequency >3 were selected for calculation in (C). **(E)** The top 15 and bottom 15 neurons among 121 neurons according to the mean expression levels of c1.up.signature and c4.up.signature in Neuron.O. **(F)** The top 15 and bottom 15 neurons among 121 neurons according to the mean expression levels of c1.up.signature and c4.up.signature in Neuron.O.T.

**Figure 4. The responses of Crh neurons to long-term 17α-estradiol treatment. (A)** The two intersected neurons among the top 10 neurons according to the mean expression levels of the three senescence-related pathways. **(B)** The expression profiles of selected pathways from the two opposing signaling networks in Neuron *Crh*, *Nppa* and *Nppc*. Neuron *Crh* and *Nppa* were the only two types of neurons shared by the three top 10 neurons in (A). **(C)** The downregulated and upregulated DEGs expressed by mitochondria or in pathway adherens junction between O.T and O in Crh neurons. **(D)** The top 25 TF activities in *Crh* and *Gnrh1* neurons. **(E)** Enzyme immunoassay of the serum levels of Crh, cortisol, and aldosterone in Y, O and O.T. Two-tail unpaired T-test was performed. p values were labeled.

**Figure 5. The response of Oxt neurons to 17α-estradiol and the causal effects of Oxt on other endocrine factors.**

**(A), (B)** The top 10 (arrows) and bottom 10 (arrows) types of neurons from 121 subtypes ranked in cell proportions among three groups. **(C)** Dot plots showing the expression profiles of the selected pathways from the two opposing signaling pathways in four types of food uptake-related neurons, which decreased or increased among the top 10 ranks in (A) or (B). Blue arrows: c1.up.signature and c4.up.signature. **(D)** Volcanic plots showing the DEGs between Neuron.O.T and Neuron.O in the pathway synaptic membrane. **(E)** Enzyme immunoassay of the plasma levels of Oxt in three groups. **(F)** Top 25 TF activities in neuron Oxt. **(G)** Significant causal effects ($p < 0.05$, IVW) between exposure OXT (id: prot-a-2159) and 203 endocrine-related outcomes, which were not significant in reverse MR analysis. Significant heterogeneity (Q_pval < 0.05). Significant horizontal pleiotropy (pval < 0.05).

**Figure 6. The response of HPG axis in the males to 17α-estradiol and the causal effects of Gnrh on other endocrine factors. (A)** The expression profiles of pathways from the two opposing signaling networks in Gnrh1-, Esr2-, Esr1- or Ar-positive neurons. **(B)** Enzyme immunoassay of the serum levels of Gnrh, bioavailable testosterone (T), and estrogen (E) in Y, O and O.T samples. Two-tail unpaired T-test was performed. **(C)** Inflammation of seminiferous tubules in testes of O and O.T. Left two panels: representative Hematoxylin–Eosin (HE) staining

of testis inflammation in O and the normal seminiferous tubules of O.T. Right panel: the mean testis inflammation index of O and O.T. **(D)** The top 25 TF activities in Gnrh1 neurons in three groups. **(E)** The activities of 14 pathways in Gnrh1-, Esr2-, Esr1- or Ar-positive neurons. **(F)** Significant causal effects (IVW, $p < 0.05$) between exposure GNRH1 (id: prot-a-1233) and 203 endocrine-related outcomes, which were not significant in reverse MR analysis. **(G)** Items with significant causal effects (IVW, $p < 0.05$) in both directions of MR analysis between GNRH1 (id: prot-a-1233) and 203 endocrine-related outcomes.

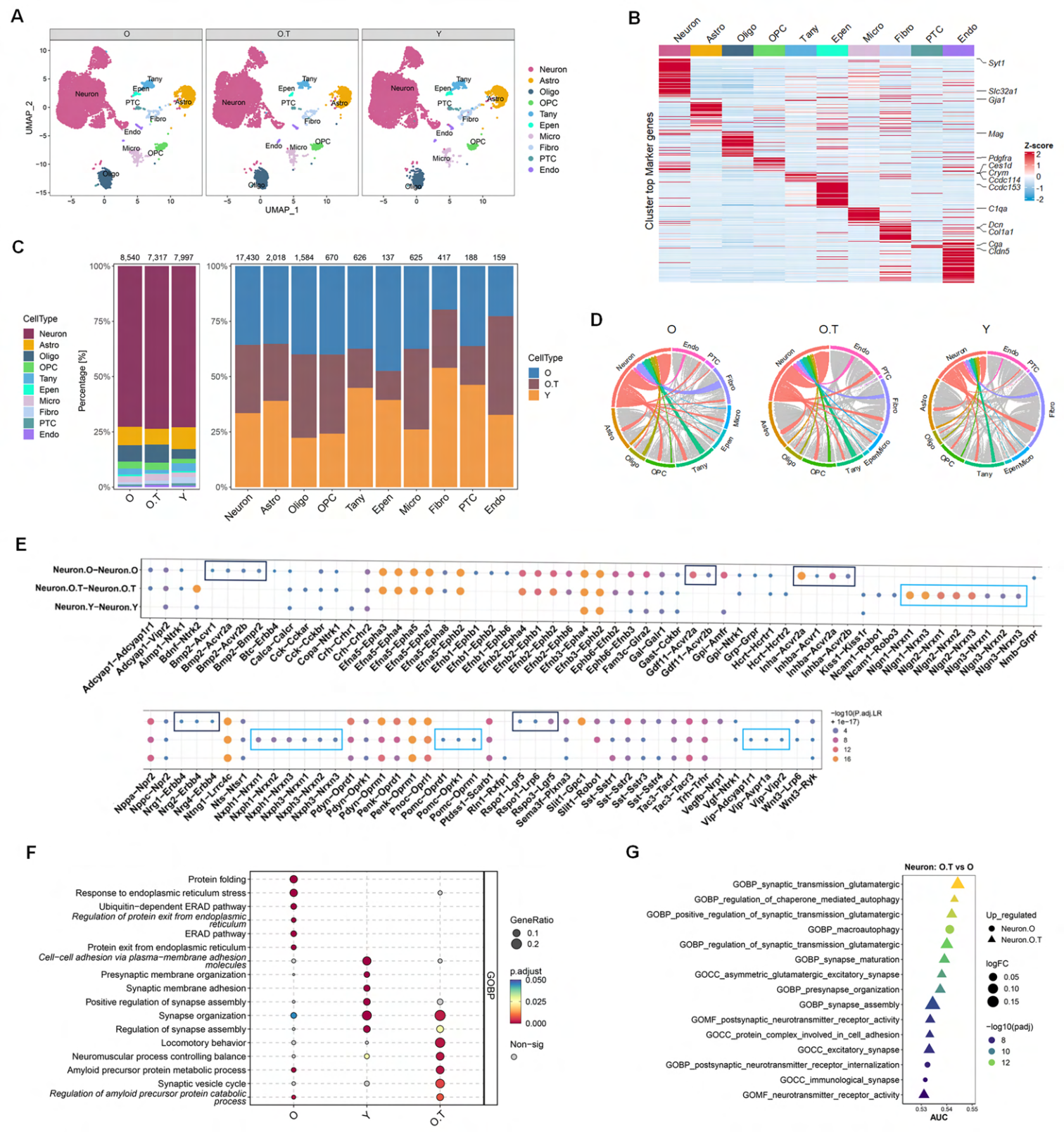
A
O
O.T
Y
UMAP_1
UMAP_2
Neuron
Astro
Oligo
OPC
Tany
Epen
Micro
Fibro
PTC
Endo
B
Cluster top Marker genes
Z-score
Syt1
Slc32a1
Gja1
Mag
Pdgfra
Ces1d
Crym
Ccdc114
Ccdc153
C1qa
Dcn
Col1a1
Cga
Cldn5
C
CellType
Percentage [%]
8,540
7,317
7,997
17,430
2,018
1,584
670
626
137
625
417
188
159
D
E
Neuron.O−Neuron.O
Neuron.O.T−Neuron.O.T
Neuron.Y−Neuron.Y
−log10(P.adj.LR + 1e−17)
F
Protein folding
Response to endoplasmic reticulum stress
Ubiquitin−dependent ERAD pathway
Regulation of protein exit from endoplasmic reticulum
ERAD pathway
Protein exit from endoplasmic reticulum
Cell−cell adhesion via plasma−membrane adhesion molecules
Presynaptic membrane organization
Synaptic membrane adhesion
Positive regulation of synapse assembly
Synapse organization
Regulation of synapse assembly
Locomotory behavior
Neuromuscular process controlling balance
Amyloid precursor protein metabolic process
Synaptic vesicle cycle
Regulation of amyloid precursor protein catabolic process
GOBP
GeneRatio
p.adjust
Non−sig
G
Neuron: O.T vs O
GOBP_synaptic_transmission_glutamatergic
GOBP_regulation_of_chaperone_mediated_autophagy
GOBP_positive_regulation_of_synaptic_transmission_glutamatergic
GOBP_macroautophagy
GOBP_regulation_of_synaptic_transmission_glutamatergic
GOBP_synapse_maturation
GOCC_asymmetric_glutamatergic_excitatory_synapse
GOBP_presynapse_organization
GOBP_synapse_assembly
GOMF_postsynaptic_neurotransmitter_receptor_activity
GOCC_protein_complex_involved_in_cell_adhesion
GOCC_excitatory_synapse
GOBP_postsynaptic_neurotransmitter_receptor_internalization
GOCC_immunological_synapse
GOMF_neurotransmitter_receptor_activity
AUC
Up_regulated
Neuron.O
Neuron.O.T
logFC
−log10(padj)

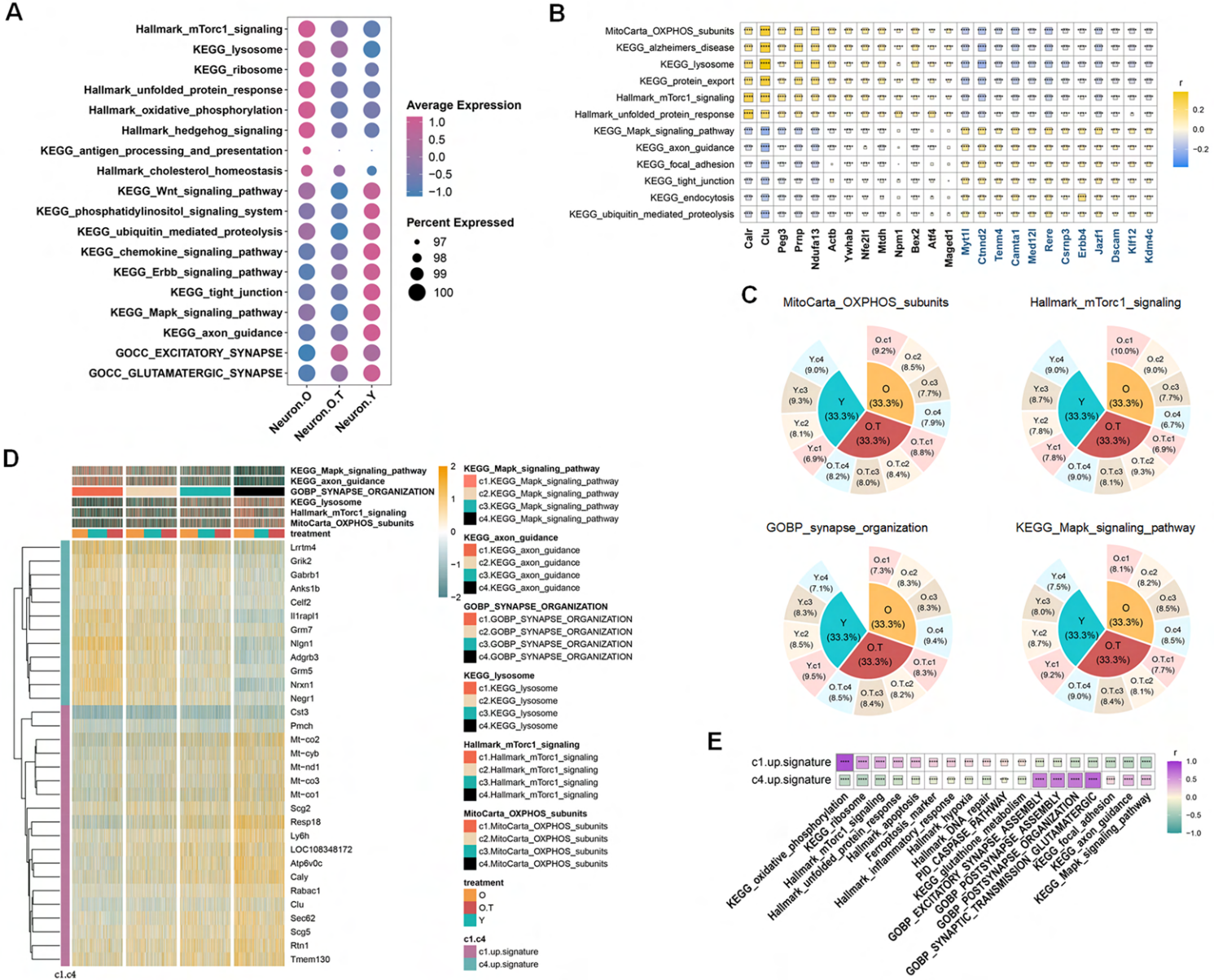
A
Hallmark_mTorc1_signaling
KEGG_lysosome
KEGG_ribosome
Hallmark_unfolded_protein_response
Hallmark_oxidative_phosphorylation
Hallmark_hedgehog_signaling
KEGG_antigen_processing_and_presentation
Hallmark_cholesterol_homeostasis
KEGG_Wnt_signaling_pathway
KEGG_phosphatidylinositol_signaling_system
KEGG_ubiquitin_mediated_proteolysis
KEGG_chemokine_signaling_pathway
KEGG_Erbb_signaling_pathway
KEGG_tight_junction
KEGG_Mapk_signaling_pathway
KEGG_axon_guidance
GOCC_EXCITATORY_SYNAPSE
GOCC_GLUTAMATERGIC_SYNAPSE
Neuron.O
Neuron.O.T
Neuron.Y
Average Expression
1.0
0.5
0.0
−0.5
−1.0
Percent Expressed
97
98
99
100
B
MitoCarta_OXPHOS_subunits
KEGG_alzheimers_disease
KEGG_lysosome
KEGG_protein_export
Hallmark_mTorc1_signaling
Hallmark_unfolded_protein_response
KEGG_Mapk_signaling_pathway
KEGG_axon_guidance
KEGG_focal_adhesion
KEGG_tight_junction
KEGG_endocytosis
KEGG_ubiquitin_mediated_proteolysis
Calr
Clu
Peg3
Prnp
Ndufa13
Actb
Ywhab
Nfe2l1
Mtdh
Npm1
Bex2
Atf4
Maged1
Myt1l
Ctnnd2
Tenm4
Camta1
Med12l
Rere
Csrnp3
Erbb4
Jazf1
Dscam
Klf12
Kdm4c
r
0.2
0.0
−0.2
C
MitoCarta_OXPHOS_subunits
Hallmark_mTorc1_signaling
GOBP_synapse_organization
KEGG_Mapk_signaling_pathway
O
(33.3%)
O.T
(33.3%)
Y
(33.3%)
D
KEGG_Mapk_signaling_pathway
KEGG_axon_guidance
GOBP_SYNAPSE_ORGANIZATION
KEGG_lysosome
Hallmark_mTorc1_signaling
MitoCarta_OXPHOS_subunits
treatment
Lrrtm4
Grik2
Gabrb1
Anks1b
Celf2
Il1rapl1
Grm7
Nlgn1
Adgrb3
Grm5
Nrxn1
Negr1
Cst3
Pmch
Mt−co2
Mt−cyb
Mt−nd1
Mt−co3
Mt−co1
Scg2
Resp18
Ly6h
LOC108348172
Atp6v0c
Caly
Rabac1
Clu
Sec62
Scg5
Rtn1
Tmem130
c1.c4
c1.KEGG_Mapk_signaling_pathway
c2.KEGG_Mapk_signaling_pathway
c3.KEGG_Mapk_signaling_pathway
c4.KEGG_Mapk_signaling_pathway
c1.KEGG_axon_guidance
c2.KEGG_axon_guidance
c3.KEGG_axon_guidance
c4.KEGG_axon_guidance
c1.GOBP_SYNAPSE_ORGANIZATION
c2.GOBP_SYNAPSE_ORGANIZATION
c3.GOBP_SYNAPSE_ORGANIZATION
c4.GOBP_SYNAPSE_ORGANIZATION
c1.KEGG_lysosome
c2.KEGG_lysosome
c3.KEGG_lysosome
c4.KEGG_lysosome
c1.Hallmark_mTorc1_signaling
c2.Hallmark_mTorc1_signaling
c3.Hallmark_mTorc1_signaling
c4.Hallmark_mTorc1_signaling
c1.MitoCarta_OXPHOS_subunits
c2.MitoCarta_OXPHOS_subunits
c3.MitoCarta_OXPHOS_subunits
c4.MitoCarta_OXPHOS_subunits
O
O.T
Y
c1.up.signature
c4.up.signature
E
c1.up.signature
c4.up.signature
KEGG_oxidative_phosphorylation
KEGG_ribosome
Hallmark_mTorc1_signaling
Hallmark_Unfolded_protein_response
Hallmark_apoptosis
Ferroptosis_marker
Hallmark_inflammatory_response
Hallmark_hypoxia
Hallmark_DNA_repair
PID_CASPASE_PATHWAY
KEGG_glutathione_metabolism
GOBP_EXCITATORY_SYNAPSE_ASSEMBLY
GOBP_POSTSYNAPSE_ASSEMBLY
GOBP_POSTSYNAPSE_ORGANIZATION
GOBP_SYNAPTIC_TRANSMISSION_GLUTAMATERGIC
KEGG_focal_adhesion
KEGG_axon_guidance
KEGG_Mapk_signaling_pathway
r
1.0
0.5
0.0
−0.5
−1.0

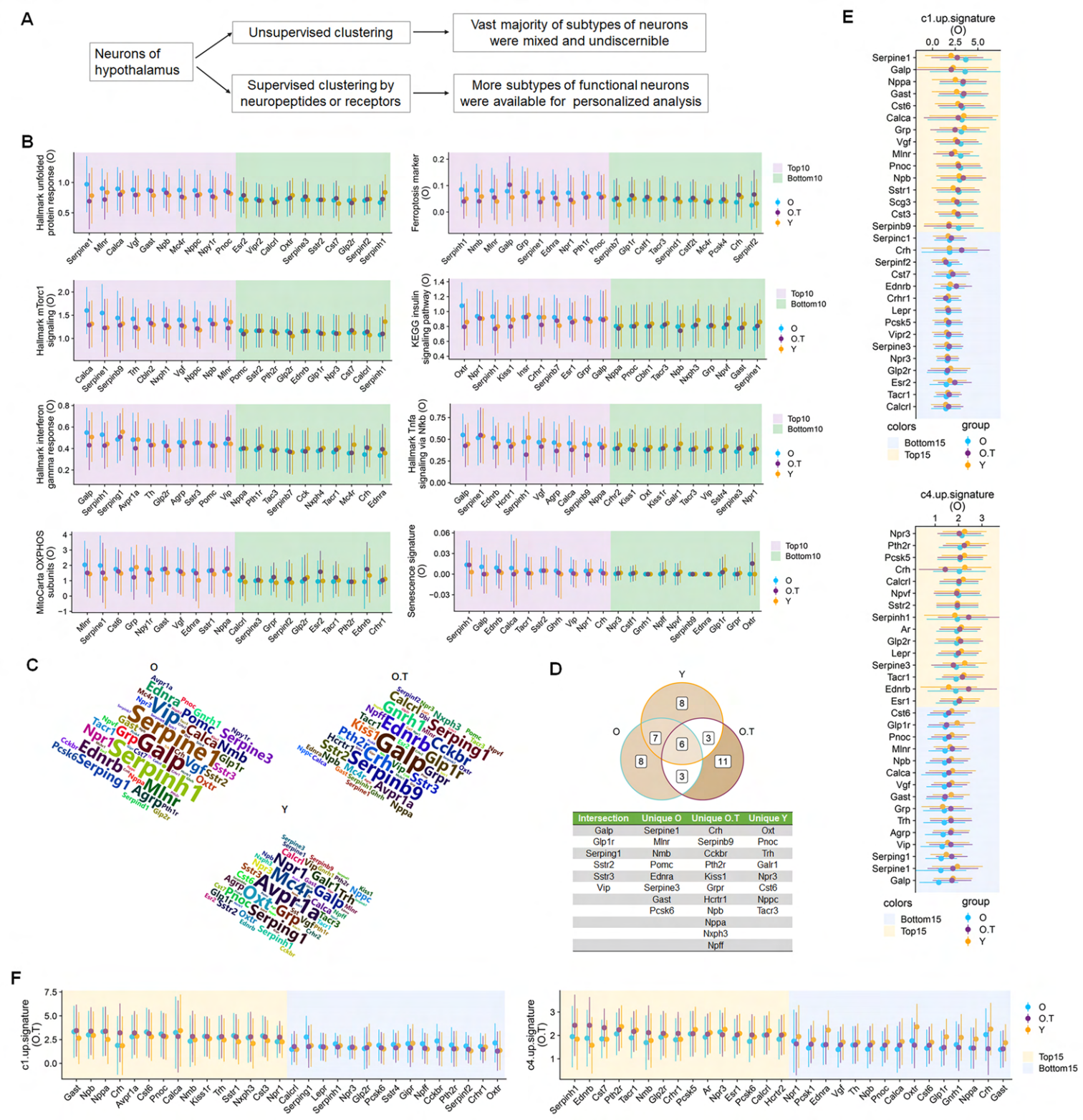
A
Neurons of hypothalamus
Unsupervised clustering
Vast majority of subtypes of neurons were mixed and undiscernible
Supervised clustering by neuropeptides or receptors
More subtypes of functional neurons were available for personalized analysis
B
Hallmark unfolded protein response (O)
Ferroptosis marker (O)
Hallmark mTorc1 signaling (O)
KEGG insulin signaling pathway (O)
Hallmark interferon gamma response (O)
Hallmark Tnfa signaling via NFkb (O)
MitoCarta OXPHOS subunits (O)
Senescence signature (O)
Top10
Bottom10
O
O.T
Y
C
O
O.T
Y
D
Y
O
O.T
8
7
6
3
8
11
3
Intersection | Unique O | Unique O.T | Unique Y
Galp | Serpine1 | Crh | Oxt
Glp1r | Mlnr | Serpinb9 | Pnoc
Serping1 | Nmb | Cckbr | Trh
Sstr2 | Pomc | Pth2r | Galr1
Sstr3 | Ednra | Kiss1 | Npr3
Vip | Serpine3 | Grpr | Cst6
Gast | Hcrtr1 | Nppc
Pcsk6 | Npb | Tacr3
Nppa
Nxph3
Npff
E
c1.up.signature (O)
0.0
2.5
5.0
Serpine1
Galp
Nppa
Gast
Cst6
Calca
Grp
Vgf
Mlnr
Pnoc
Npb
Sstr1
Scg3
Cst3
Serpinb9
Serpinc1
Crh
Serpinf2
Cst7
Ednrb
Crhr1
Lepr
Pcsk5
Vipr2
Serpine3
Npr3
Glp2r
Esr2
Tacr1
Calcrl
colors
group
Bottom15
Top15
O
O.T
Y
c4.up.signature (O)
1
2
3
Npr3
Pth2r
Pcsk5
Crh
Calcrl
Npvf
Sstr2
Serpinh1
Ar
Glp2r
Lepr
Serpine3
Tacr1
Ednrb
Esr1
Cst6
Glp1r
Pnoc
Mlnr
Npb
Calca
Vgf
Gast
Grp
Trh
Agrp
Vip
Serping1
Serpine1
Galp
colors
group
Bottom15
Top15
O
O.T
Y
F
c1.up.signature (O.T)
7.5
5.0
2.5
0.0
Gast
Npb
Nppa
Crh
Avpr1a
Cst6
Pnoc
Calca
Nmb
Kiss1r
Trh
Sstr1
Nxph3
Cst3
Npr1
Calcrl
Serping1
Lepr
Serpinh1
Npr3
Glp2r
Pcsk6
Sstr4
Grpr
Npff
Cckbr
Pth2r
Serpinf2
Crhr1
Oxtr
c4.up.signature (O.T)
3
2
1
Serpinh1
Ednrb
Cst7
Pth2r
Tacr1
Nmb
Glp2r
Crhr1
Pcsk5
Ar
Npr3
Esr1
Pcsk6
Calcrl
Hcrtr2
Npr1
Pcsk1
Ednra
Vgf
Trh
Npb
Pnoc
Calca
Oxtr
Cst6
Glp1r
Gnrh1
Nppa
Crh
Gast
O
O.T
Y
Top15
Bottom15

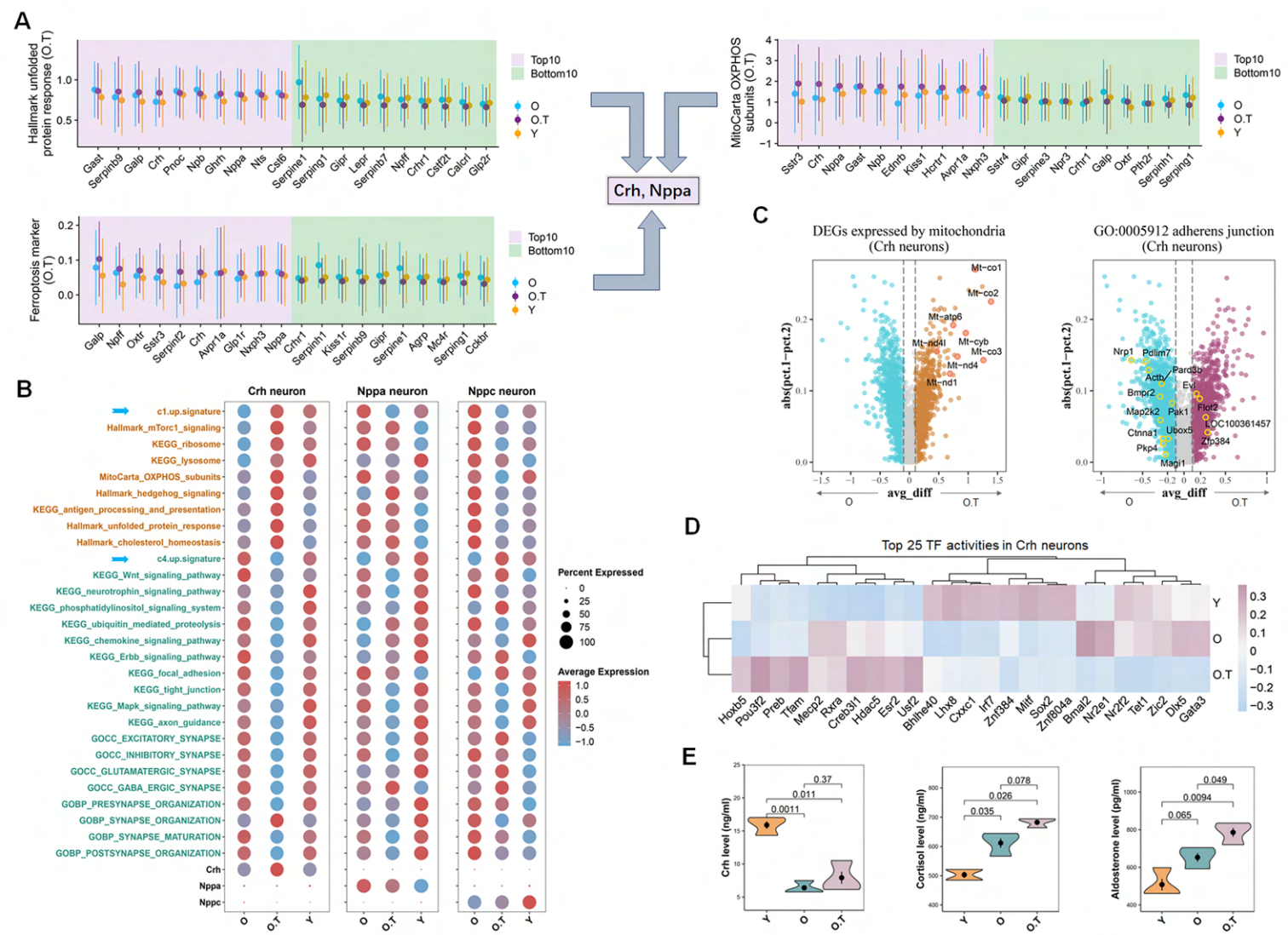
A
Hallmark unfolded protein response (O.T)
Top10
Bottom10
O
O.T
Y
Gast Serpinb9 Galp Crh Pnoc Npb Ghrh Nppa Nts Cst6 Serpine1 Serping1 Gipr Lepr Serpinb7 Npff Crhr1 Cstf2t Calcr1 Glp2r
MitoCarta OXPHOS subunits (O.T)
Sstr3 Crh Nppa Gast Npb Ednrb Kiss1 Hcrtr1 Avpr1a Nxph3 Sstr4 Gipr Serpine3 Npr3 Crhr1 Galp Oxtr Pth2r Serpinh1 Serping1
Ferroptosis marker (O.T)
Galp Npff Oxtr Sstr3 Serpinf2 Crh Avpr1a Glp1r Nxph3 Nppa Crhr1 Serpinh1 Kiss1r Serpinb9 Gipr Serpine1 Agrp Mc4r Serping1 Cckbr
Crh, Nppa
B
Crh neuron
Nppa neuron
Nppc neuron
c1.up.signature
Hallmark_mTorc1_signaling
KEGG_ribosome
KEGG_lysosome
MitoCarta_OXPHOS_subunits
Hallmark_hedgehog_signaling
KEGG_antigen_processing_and_presentation
Hallmark_unfolded_protein_response
Hallmark_cholesterol_homeostasis
c4.up.signature
KEGG_Wnt_signaling_pathway
KEGG_neurotrophin_signaling_pathway
KEGG_phosphatidylinositol_signaling_system
KEGG_ubiquitin_mediated_proteolysis
KEGG_chemokine_signaling_pathway
KEGG_Erbb_signaling_pathway
KEGG_focal_adhesion
KEGG_tight_junction
KEGG_Mapk_signaling_pathway
KEGG_axon_guidance
GOCC_EXCITATORY_SYNAPSE
GOCC_INHIBITORY_SYNAPSE
GOCC_GLUTAMATERGIC_SYNAPSE
GOCC_GABA_ERGIC_SYNAPSE
GOBP_PRESYNAPSE_ORGANIZATION
GOBP_SYNAPSE_ORGANIZATION
GOBP_SYNAPSE_MATURATION
GOBP_POSTSYNAPSE_ORGANIZATION
Crh
Nppa
Nppc
Percent Expressed
Average Expression
C
DEGs expressed by mitochondria (Crh neurons)
GO:0005912 adherens junction (Crh neurons)
abs(pct.1−pct.2)
avg_diff
O
O.T
Mt-co1
Mt-co2
Mt-atp6
Mt-nd4l
Mt-cyb
Mt-co3
Mt-nd4
Mt-nd1
Nrp1
Pdlim7
Pard3b
Actb
Evl
Bmpr2
Flot2
Map2k2
Pak1
LOC100361457
Ctnna1
Ubox5
Zfp384
Pkp4
Magi1
D
Top 25 TF activities in Crh neurons
Hoxb5 Pou3f2 Preb Tfam Mecp2 Rxra Creb3l1 Hdac5 Esr2 Usf2 Bhlhe40 Lhx8 Cxxc1 Irf7 Znf384 Mitf Sox2 Znf804a Bmal2 Nr2e1 Nr2f2 Tet1 Zic2 Dlx5 Gata3
E
Crh level (ng/ml)
Cortisol level (ng/ml)
Aldosterone level (pg/ml)
0.37
0.011
0.0011
0.078
0.026
0.035
0.049
0.0094
0.065

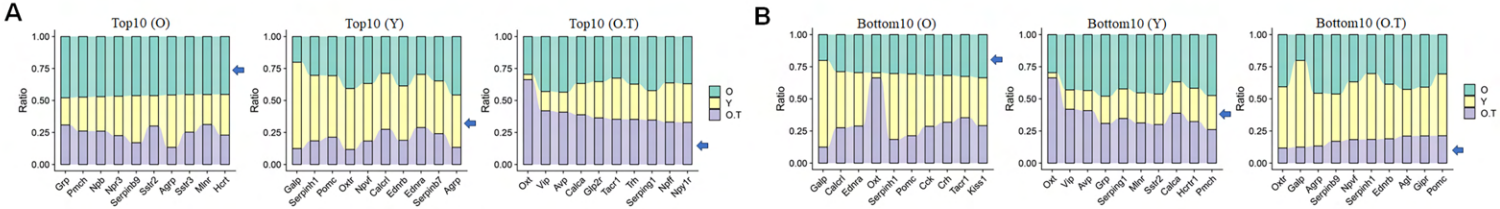


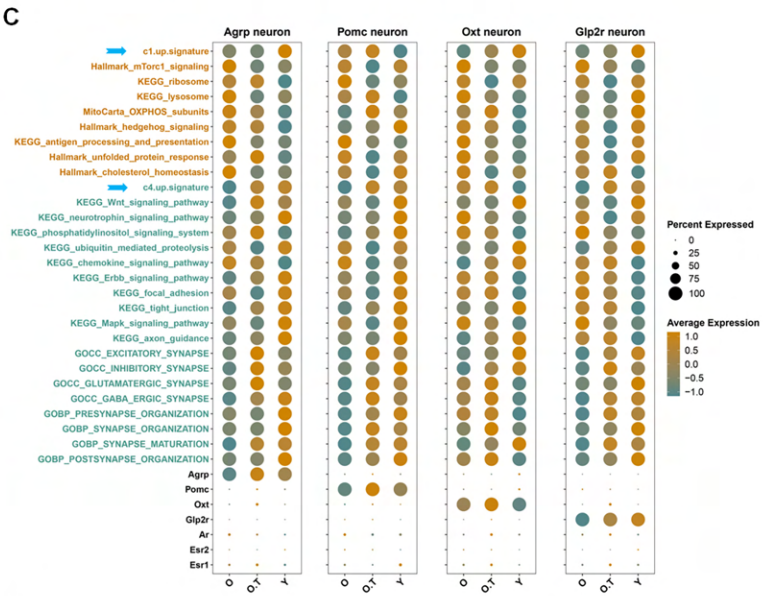


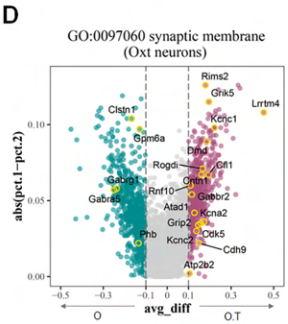


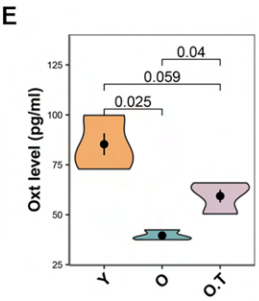


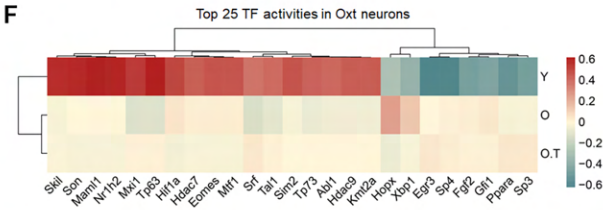


G

| outcome | method | nsnp | OR(95%CI) | pval | Q_pval | pleiotropy.pval |
|---|---|---|---|---|---|---|
| Neurexophilin−1 \|\| id:prot−a−2132 | IVW | 34 | 1.327 (1.223 to 1.439) | 1e−11 | 0.12 | 0.05 |
| Amyloid−like protein 2 \|\| id:prot−a−123 | IVW | 34 | 1.264 (1.176 to 1.359) | 2.4e−10 | 0.42 | 0.2 |
| Pro−opiomelanocortin \|\| id:prot−a−2327 | IVW | 68 | 1.147 (1.090 to 1.207) | 1.6e−07 | 0.42 | 0.46 |
| Agouti−signaling protein \|\| id:prot−a−187 | IVW | 68 | 0.882 (0.837 to 0.930) | 2.7e−06 | 0.32 | 0.11 |
| Glucagon \|\| id:prot−a−1181 | IVW | 34 | 1.124 (1.046 to 1.207) | 0.0014 | 0.86 | 0.35 |
| Insulin−like growth factor−binding protein 2 \|\| id:prot−a−1448 | IVW | 34 | 1.124 (1.040 to 1.215) | 0.0033 | 0.21 | 0.8 |
| Cystatin C levels \|\| id:ebi−a−GCST90025945 | IVW | 5 | 1.020 (1.006 to 1.035) | 0.0045 | 0.54 | 0.88 |
| Cystatin−F \|\| id:prot−a−705 | IVW | 34 | 1.108 (1.031 to 1.190) | 0.005 | 0.75 | 0.43 |
| Cerebellin−1 \|\| id:prot−a−371 | IVW | 34 | 0.899 (0.835 to 0.969) | 0.0053 | 0.33 | 0.87 |
| Neuropeptide W \|\| id:prot−a−2082 | IVW | 68 | 0.932 (0.886 to 0.980) | 0.006 | 0.98 | 0.31 |
| Glial cell line−derived neurotrophic factor \|\| id:prot−a−1198 | IVW | 34 | 1.105 (1.023 to 1.194) | 0.011 | 0.24 | 0.57 |
| Serpin A9 \|\| id:prot−a−2694 | IVW | 34 | 1.113 (1.024 to 1.210) | 0.012 | 0.078 | 0.4 |
| Beta−endorphin \|\| id:prot−a−2325 | IVW | 34 | 1.123 (1.025 to 1.229) | 0.012 | 0.015 | 0.78 |
| Total testosterone levels \|\| id:ebi−a−GCST90012112 | IVW | 33 | 1.012 (1.002 to 1.021) | 0.015 | 0.13 | 0.97 |
| Thyroid Stimulating Hormone \|\| id:prot−a−530 | IVW | 34 | 1.092 (1.016 to 1.172) | 0.016 | 0.75 | 0.58 |
| Progonadoliberin−1 \|\| id:prot−a−1233 | IVW | 34 | 1.091 (1.016 to 1.172) | 0.017 | 0.82 | 0.42 |
| Insulin−like growth factor 1 levels \|\| id:ebi−a−GCST90025989 | IVW | 5 | 0.984 (0.970 to 0.998) | 0.025 | 0.71 | 0.29 |
| Total Testosterone \|\| id:ieu−b−4864 | IVW | 32 | 1.011 (1.001 to 1.020) | 0.026 | 0.52 | 0.92 |
| Thyroid hormone receptor alpha \|\| id:prot−a−2974 | IVW | 34 | 1.085 (1.003 to 1.173) | 0.041 | 0.2 | 0.56 |
| Insulin−like growth factor−binding protein 1 levels \|\| id:ebi−a−GCST90010221 | IVW | 30 | 1.148 (1.006 to 1.311) | 0.041 | 0.29 | 0.92 |
| Insulin−like 3 \|\| id:prot−a−1560 | IVW | 34 | 1.106 (1.003 to 1.218) | 0.043 | 0.0022 | 0.82 |
| Growth hormone receptor \|\| id:prot−a−1211 | IVW | 68 | 0.941 (0.887 to 0.999) | 0.046 | 0.019 | 0.26 |

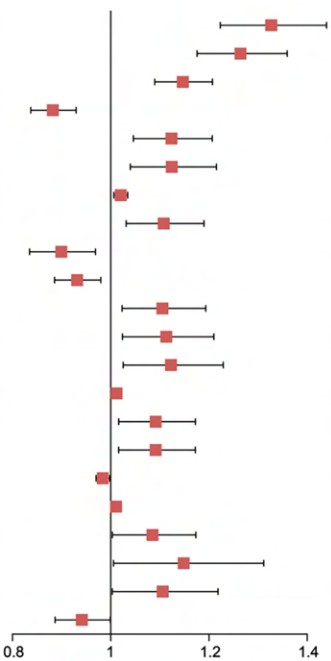

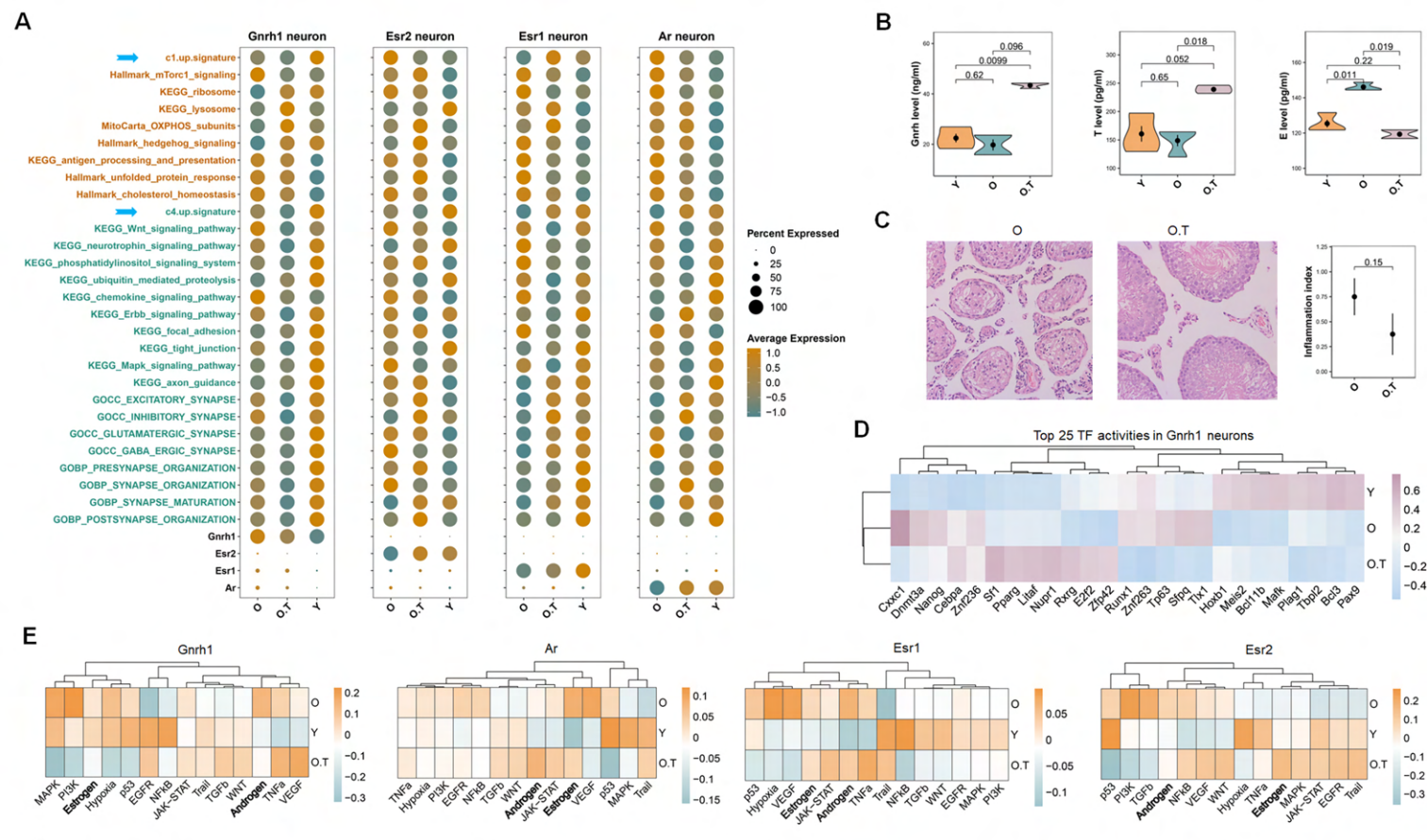


F

| exposure | outcome | method | nsnp | OR(95%CI) | pval | Q_pval | pleiotropy.pval |
|---|---|---|---|---|---|---|---|
| GNRH1 | Proenkephalin−A \|\| id:prot−a−2247 | IVW | 48 | 1.336 (1.264 to 1.413) | 1.9e−24 | 0.72 | 0.26 |
| GNRH1 | Proprotein convertase subtilisin/kexin type 7 \|\| id:prot−a−2212 | IVW | 24 | 1.254 (1.159 to 1.357) | 1.8e−08 | 0.51 | 0.95 |
| GNRH1 | Agouti−signaling protein \|\| id:prot−a−187 | IVW | 48 | 1.218 (1.132 to 1.310) | 1.3e−07 | 0.0015 | 0.31 |
| GNRH1 | Growth hormone receptor \|\| id:prot−a−1211 | IVW | 48 | 0.863 (0.816 to 0.913) | 2.3e−07 | 0.98 | 0.34 |
| GNRH1 | Galanin peptides \|\| id:prot−a−1166 | IVW | 24 | 1.236 (1.133 to 1.349) | 1.9e−06 | 0.2 | 0.93 |
| GNRH1 | Estrogen receptor \|\| id:prot−a−991 | IVW | 24 | 1.222 (1.124 to 1.329) | 2.8e−06 | 0.3 | 0.73 |
| GNRH1 | Pro−opiomelanocortin \|\| id:prot−a−2327 | IVW | 48 | 1.139 (1.077 to 1.204) | 4.8e−06 | 0.98 | 0.083 |
| GNRH1 | Insulin−like growth factor−binding protein 6 \|\| id:prot−a−1450 | IVW | 24 | 1.232 (1.124 to 1.351) | 8.7e−06 | 0.11 | 0.67 |
| GNRH1 | Beta−endorphin \|\| id:prot−a−2325 | IVW | 24 | 1.184 (1.094 to 1.281) | 0.000027 | 0.55 | 0.48 |
| GNRH1 | Brain−derived neurotrophic factor \|\| id:prot−a−242 | IVW | 24 | 1.131 (1.045 to 1.223) | 0.0022 | 0.63 | 0.91 |
| GNRH1 | Adrenomedullin \|\| id:prot−a−48 | IVW | 24 | 1.271 (1.083 to 1.492) | 0.0033 | 9.3e−11 | 0.72 |
| GNRH1 | Insulin−like growth factor−binding protein 1 levels \|\| id:ebi−a−GCST90010221 | IVW | 22 | 0.820 (0.718 to 0.936) | 0.0034 | 0.28 | 0.57 |
| GNRH1 | Prolactin receptor \|\| id:prot−a−2377 | IVW | 24 | 1.124 (1.039 to 1.216) | 0.0036 | 0.85 | 0.44 |
| GNRH1 | Insulin−like growth factor−binding protein 3 \|\| id:prot−a−1449 | IVW | 24 | 0.883 (0.811 to 0.962) | 0.0044 | 0.25 | 0.63 |
| GNRH1 | Early placenta insulin−like peptide \|\| id:prot−a−1561 | IVW | 24 | 1.117 (1.032 to 1.208) | 0.0059 | 0.58 | 0.58 |
| GNRH1 | Bradykinin, des−arg(9) \|\| id:met−a−656 | IVW | 10 | 0.778 (0.641 to 0.943) | 0.01 | 4.6e−31 | 0.071 |
| GNRH1 | Leptin receptor \|\| id:prot−a−1724 | IVW | 24 | 1.097 (1.014 to 1.187) | 0.021 | 0.98 | 0.42 |
| GNRH1 | Thyroid hormone receptor alpha \|\| id:prot−a−2974 | IVW | 24 | 1.086 (1.004 to 1.176) | 0.039 | 0.82 | 0.78 |

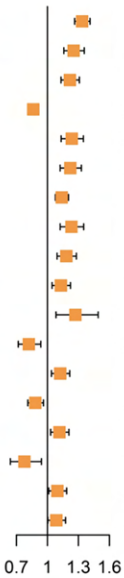


G
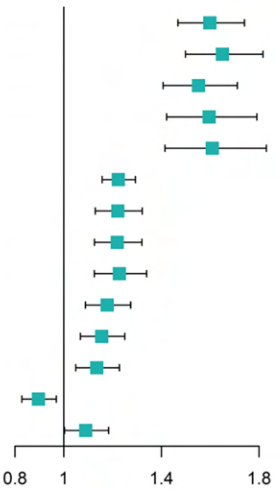
| exposure | outcome | method | nsnp | OR(95%CI) | pval | Q_pval | pleiotropy.pval |
|---|---|---|---|---|---|---|---|
| GNRH1 | Somatostatin−28 \|\| id:prot−a−2846 | IVW | 24 | 1.598 (1.468 to 1.740) | 4.1e−27 | 0.26 | 0.53 |
| GNRH1 | Chromogranin−A \|\| id:prot−a−538 | IVW | 24 | 1.650 (1.499 to 1.816) | 1.7e−24 | 0.06 | 0.5 |
| GNRH1 | Neuropeptide W \|\| id:prot−a−2082 | IVW | 48 | 1.552 (1.407 to 1.711) | 1.3e−18 | 4.8e−12 | 0.77 |
| GNRH1 | Protachykinin−1 \|\| id:prot−a−2920 | IVW | 24 | 1.596 (1.421 to 1.791) | 2.3e−15 | 0.001 | 0.89 |
| GNRH1 | Glucagon \|\| id:prot−a−1181 | IVW | 24 | 1.609 (1.414 to 1.830) | 4.5e−13 | 0.000021 | 0.98 |
| GNRH1 | Brain natriuretic peptide 32 \|\| id:prot−a−2077 | IVW | 48 | 1.223 (1.157 to 1.294) | 1.3e−12 | 0.9 | 0.026 |
| GNRH1 | Corticotropin \|\| id:prot−a−2326 | IVW | 24 | 1.221 (1.129 to 1.322) | 6.4e−07 | 0.79 | 0.73 |
| GNRH1 | Prolactin−releasing peptide \|\| id:prot−a−2376 | IVW | 24 | 1.219 (1.126 to 1.320) | 1.1e−06 | 0.43 | 0.089 |
| GNRH1 | Progonadoliberin−2 \|\| id:prot−a−1234 | IVW | 24 | 1.228 (1.125 to 1.340) | 4e−06 | 0.21 | 0.42 |
| GNRH1 | Secretogranin−1 \|\| id:prot−a−539 | IVW | 24 | 1.178 (1.089 to 1.274) | 0.000046 | 0.81 | 0.51 |
| GNRH1 | Atrial natriuretic factor \|\| id:prot−a−2076 | IVW | 24 | 1.155 (1.068 to 1.250) | 0.00032 | 0.57 | 0.56 |
| GNRH1 | Estradiol 17−beta−dehydrogenase 2 \|\| id:prot−a−1383 | IVW | 24 | 1.135 (1.049 to 1.228) | 0.0016 | 0.69 | 0.62 |
| GNRH1 | Insulin−like growth factor I \|\| id:prot−a−1443 | IVW | 24 | 0.896 (0.828 to 0.970) | 0.0063 | 0.95 | 0.48 |
| GNRH1 | Insulin−like growth factor 1 receptor \|\| id:prot−a−1444 | IVW | 24 | 1.090 (1.003 to 1.184) | 0.042 | 0.33 | 0.62 |